

LA-UR-15-22679 (Accepted Manuscript)

Precise relative locations for earthquakes in the northeast Pacific region

Cleveland, Kenneth Michael Ammon, Charles VanDeMark, Thomas

Provided by the author(s) and the Los Alamos National Laboratory (2016-05-03).

To be published in: Journal of Geophysical Research: Solid Earth

DOI to publisher's version: 10.1002/2015JB012161

Permalink to record: http://permalink.lanl.gov/object/view?what=info:lanl-repo/lareport/LA-UR-15-22679

Disclaimer

Approved for public release. Los Alamos National Laboratory, an affirmative action/equal opportunity employer, is operated by the Los Alamos National Security, LLC for the National Nuclear Security Administration of the U.S. Department of Energy under contract DE-AC52-06NA25396. Los Alamos National Laboratory strongly supports academic freedom and a researcher's right to publish; as an institution, however, the Laboratory does not endorse the viewpoint of a publication or guarantee its technical correctness.



Precise Relative Locations for Earthquakes in the Northeast Pacific Region

K. Michael Cleveland¹, Thomas F. VanDeMark², Charles J. Ammon³

¹Los Alamos National Laboratory, EES-17: Geophysics, Los Alamos, NM 87545

²Air Force Technical Applications Center, Patrick Air Force Base, FL, USA

³ The Pennsylvania State University, Department of Geosciences, University Park, PA 16802

Submitted to Journal of Geophysical Research

K. Michael Cleveland EES-17: Geophysics LANL Mail Station D446 P.O. Box 1663 Los Alamos, NM, 87545 mike.cleveland@gmail.com

1 **Abstract**

2

3

4

5

6

7

8

9

10

11

12

13

14

15

16

17

18

19

20

21

Double-difference methods applied to cross-correlation measured Rayleigh wave time shifts are an effective tool to improve epicentroid locations and relative origin-time shifts in remote regions. We apply these methods to seismicity offshore of southwestern Canada and the U.S. Pacific Northwest, occurring along the boundaries of the Pacific and Juan de Fuca (including the Explorer plate and Gorda block) plates. The Blanco, Mendocino, Revere-Dellwood, Nootka, and Sovanco fracture zones host the majority of this seismicity, largely consisting of strike-slip earthquakes. The Explorer, Juan de Fuca, and Gorda spreading ridges join these fracture zones and host normal faulting earthquakes. Our results show that at least the moderate-magnitude activity clusters along fault strike, supporting suggestions of large variations in seismic coupling along oceanic transform faults. Our improved relative locations corroborate earlier interpretations of the internal deformation in the Explorer and Gorda plates. North of the Explorer Plate, improved locations support models that propose northern extension of the Revere-Dellwood fault. Relocations also support interpretations that favor multiple parallel active faults along the Blanco Transform Fault Zone. Seismicity of the western half of the Blanco appears more scattered and less collinear than the eastern half, possibly related to fault maturity. We use azimuthal variations in the Rayleigh-wave cross-correlation amplitude to detect and model rupture directivity for a moderate-size earthquake along the eastern Blanco fault. The observations constrain the seismogenic zone geometry and suggest a relatively narrow seismogenic zone width of 2 to 4 km.

1. Introduction

22

23

24

25

26

27

28

29

30

31

32

33

34

35

36

37

38

39

40

41

42

1.1 Global Oceanic Transform Faults

Although oceanic transform faults (OTF) constitute roughly 20% of the total global plate boundary length [Bird, 2003], their small maximum earthquake size, remoteness, and small tsunami hazard minimize their effect on humans. However, better constraints on OTF tectonic parameters (e.g. fault length, slip rate, and thermal structure) [Boettcher and Jordan, 2004] compared to other tectonic boundaries make OTFs a useful focus for the investigation of earthquake processes. In particular, OTF compositional structure is more homogeneous and OTF thermal structure is more accurately predicted than along other major plate boundaries [Turcotte and Schubert, 2002; Behn et al., 2007; Roland et al., 2010]. But important differences also exist between OTFs and other tectonic boundaries. Most OTFs appear to have relatively small maximum magnitude thresholds (M < 7.0) [e.g. Boettcher and Jordan, 2004]. Aftershocks associated with OTF earthquakes are generally fewer and smaller than those typical along other plate boundaries - the largest aftershock is usually two magnitude units smaller than the mainshock [Boettcher and Jordan, 2004]. However, transform seismicity is on average well described by a truncated Gutenberg-Richter distribution with a self-similar slope of $\beta = 2/3$ [Bird et al., 2002; Boettcher and Jordan, 2004], consistent with global averages [Stein and Wysession, 2003]. Many studies have identified strong thermal controls on the maximum seismogenic zone

depth extent for OTFs [Wiens and Stein, 1983; Engeln et al., 1986; Bergman and

51

61

Solomon, 1988; Abercrombie and Ekström, 2001; Braunmiller and Nábělek, 2008; 44 Boettcher et al., 2007]. Specifically, seismicity along OTFs appears limited to 45 temperatures less than 600°C (e.g. Abercrombie and Ekström, 2001; Braunmiller and 46 Nábělek, 2008). Modeling by Roland et al. [2010] suggests that hydrothermal cooling 47 causes thermal boundaries of the seismogenic zone to deepen more quickly near ridge-48 transform boundaries than half-space models suggest, and the seismogenic width remains 49 fairly constant over the length of the fault, particularly for longer faults and slower slip 50 rates. In addition, hydrothermal alteration of the mantle may extend the depth of brittle deformation [Roland et al., 2010]. 52 The relative deficiency in cumulative seismic moment along OTFs suggests that OTFs 53 generally have low seismic coupling (e.g. Brune, 1968; Davies and Brune, 1971; Frohlich 54 and Apperson, 1992; Okal and Langenhorst, 2000). Bird et al. [2002] noted the difficulty 55 in identifying any fully-coupled fault segments because significant slip occurs 56 aseismically along these faults. On average, OTF seismic coupling varies between 10% to 57 30%, however, coupling may vary significantly along strike [Boettcher and Jordan, 58 2004]. Earlier studies noted a decrease in coupling with spreading rate (e.g. Kawaski et 59 al., 1985, Sobolev and Rundquist, 1999; Bird et al., 2002; Rundquist and Sobolev, 2002). 60 Using estimated fault length and slip rate values, the observed rupture area of the largest OTF earthquakes is less than the total area above the inferred 600°C isotherm. Possible 62 models to explain this behavior include a thin (limited depth extent) seismogenic zone 63 with uniform coupling along strike or a wide seismogenic zone with variable coupling 64 along strike [Boettcher and Jordan, 2004].

71

81

2. Northeast Pacific Oceanic Transform Faults

Our focus area, the northeast Pacific, west of Cascadia subduction zone, is shown in 66 67 Figure 1. This region includes seismicity associated with the interaction of the Pacific. 68 Gorda, Juan de Fuca, Explorer, and North American Plates. The Gorda, Juan de Fuca, 69 and Explorer are all remnants of the Farallon Plate, which began breaking up in the 70 Tertiary [Engebretson et al., 1985; Lonsdale, 1991; Stock and Lee, 1994]. Around 30 Ma, the Farallon-Pacific spreading center reached the Farallon-North America subduction 72 zone, and the Farallon split into the Juan de Fuca Plate in the north and Nazca-Cocos in 73 the south [Stock and Molnar, 1988]. As the North America-Juan de Fuca-Pacific triple 74 junction propagated north over time, the Juan de Fuca Plate continued to decrease in size 75 and to fragment [Atwater, 1989]. In the last 5 Ma, two segments of the Juan de Fuca are 76 believed to have begun to move independently, forming the Gorda deformation zone in 77 the south [Riddihough, 1980; Wilson, 1986; 1989] and Explorer Plate in the north [Barr 78 and Chase, 1974; Riddihough, 1977; 1984; Botros and Johnson, 1988]. 79 In this study, we provide improved relative epicentroid locations and magnitudes for 80 select OTF earthquakes in the northeast Pacific region using intermediate-period (30-80 s) relative Rayleigh wave cross-correlation measurements. While many others have 82 used body waves to relocate events in this region using different methodologies (e.g. 83 Sverdrup, 1987; Stoddard and Woods, 1990; Dziak et al., 2000; Braunmiller and 84 Nábělek, 2002; Cronin and Sverdrup, 2003), only limited work has been done in this 85 region using surface waves [Boettcher and McGuire, 2009]. The relocation method we 86 employ provides particular advantage in OTF settings. Surface waves are commonly more clearly observed than body-waves at stations of greater distance, increasing the number of usable stations and expanding azimuthal coverage available for relocation. Additionally, surface waves are less sensitive to small changes in earth structure and

measurement uncertainty.

Interpreting the observed patterns and characteristics of these improved locations provides insight into the regional tectonics of the northeast Pacific region. In the Gorda and Explorer Plate, precise locations are important for identifying and analyzing internal plate deformation. Along the BTFZ, the improved locations assist in interpreting whether slip is distributed along a single or multiple active faults. As will be discussed later for the BTFZ, the improved locations also enable investigation of fault properties; this includes analysis of how seismicity changes along the length the fault, as well as estimation of the width of the seismogenic zone.

3. Methods

Multiple studies have utilized surface wave observations for earthquake location (e.g. von Seggern, 1972; Ekström, 2006; Ekström and Richards, 1994; VanDeMark, 2006; McGuire, 2008; Barmin et al., 2011; Herrmann et al., 2011; Wei et al., 2012; Cleveland and Ammon, 2013). Because they have lower propagation speeds than body waves, surface waves can provide enhanced sensitivity to event location. Precise measurement of relative surface-wave time shifts benefits from the high waveform similarity for events with similar faulting geometry and depth. Cleveland and Ammon [2013] showed that the necessary degree of similarity in faulting geometry and depth between events for oceanic

109

110

111

112

113

114

115

116

117

118

119

120

121

122

123

124

125

126

127

128

129

130

transform fault tectonic settings is functionally broad in the intermediate-period Rayleigh-wave band (30-80 s); small to moderate changes in depth and mechanisms do not significantly affect the relative location accuracy. In this study, we apply methods developed earlier (i.e. VanDeMark, 2006; Cleveland and Ammon, 2013), and combine Rayleigh-wave time-shift observations in a multiple-event, double-difference based inversion, to estimate optimal oceanic transform fault earthquake epicentroid locations in the northeast Pacific region. As described in Cleveland and Ammon [2013], the term "epicentroid" indicates the spatial average of seismic moment release sensed by signals in the period range from about 80 to 30s. We selected 125 out of 154 earthquakes in the region based on a search of the Global CMT (GCMT) catalog (e.g. Dziewonski et al., 1981: Ekström et al., 2012) for vertical strike-slip earthquakes $M_w \ge 4.5$ since 1990. The remaining events were either located too far away from surrounding events or lacked a sufficient number of viable waveforms with acceptable signal-to-noise. We also supplemented the strike-slip event set with 36 normal-faulting events (see electronic supplement). Most events have magnitudes between 4.5 and 6.5, with a mean of about M_w 5.3; however, we include events as large as M_w 7.2. We used similar data processing procedures to those described by *Cleveland and Ammon* [2013], and we focused only on short-arc Rayleigh waves (R1). We computed displacement seismograms using a frequency-domain instrument-response deconvolution. We excluded data from most temporary networks, but included US Transportable Array data (Figure 2). Seismograms were graded from A to F by visual inspection of the signal quality; only signals with quality C and better were used for our analysis. A group-velocity window (5.0 to 3.0 km/s) was used to isolate Rayleigh waves

132

133

134

135

136

137

138

139

140

141

142

143

144

145

146

147

148

149

150

151

152

153

and we filtered signals to enhance the period range 80 to 30 seconds. We used cross-correlation to estimate the average time difference for the surface waveforms between corresponding signals from each event. Using these time differences, we invert for relative centroid latitude, longitude (an epicentroid), and time of the events using a spherical-earth version of the double-difference equations of *Waldhauser and Ellsworth* [2000]. Further details of the inversion procedure can be found in *Cleveland and Ammon* [2013].

Calculation of the locations requires specification of several parameters. Criteria must be defined to determine cross-correlation significance and event linking parameters, and average, regional surface-wave slowness used to convert time-shifts to distance. The linking parameters include the maximum distance allowed between two linked events and the number of double-difference observations necessary to link two events. Cleveland and Ammon [2013] provide sensitivity tests of these parameters. With the exception of the slowness value, we use the same parameter values as this earlier study. While the correlation coefficient threshold can be set to values as low as 0.75 (cross-correlation normalized to 1.00) since we generally have good azimuthal coverage, we conservatively use a threshold of 0.90. Events were only linked for the inversion if they are located within 120 km of each other. We also introduce a linking criteria based on the azimuth distribution of stations (something not used in Cleveland and Ammon [2013]). Previously, we required at least 12 common stations with good correlation for two events to link; but if the stations are all located at a narrow azimuth region from both events, they will not provide sufficient information to characterize the variation of travel time with azimuth. In this study, we require that the largest gap in station coverage is no larger

than 310°. In other words, we require at least 50° span by the observations, which still provide enough data to reasonably constrain the azimuthal cosine pattern in relative arrival times produced by two nearby events. Application of this criterion unlinked eight events, which had very narrow azimuthal control (and thus very little control on the relative epicentroid locations of the two events). Changing the gap requirement does not significantly influence the event relocations we discuss. We compared locations calculated with a 50° limit and those without any azimuth limit and found a maximum difference in location of less than one km, and mean and median differences of 0.06 and 0.00 km. The primary effect is to remove the events that have an insufficient number of observations. Azimuthal spans significantly larger than 50° do not appreciably improve the relocation.

The misfit to the double-difference times is only slightly sensitive to average slowness values (within a range of reasonable values). We determined optimal surface-wave slowness by using the value that minimized the average misfit between the revised and original US Geological Survey NEIC locations. For the Explorer and Gorda regions, a slowness of 0.26 s/km (3.85 km/s) provided the minimum difference from the original locations. Along the BTFZ, the optimal slowness was slightly higher, 0.28 s/km (3.57 km/s). The difference between slownesses of 0.26 and 0.28 s/km expanded/contracted the event locations along strike from the center of the epicentroid cluster. The mean and maximum relocation differences between the two slownesses were about one and six km, respectively; this difference did not change the event distances normal to the fault trace. Compared with values corresponding to PREM and model GDM52 [Ekström, 2011], a

slowness of 0.26 s/km is reasonable for all three regions. For these reasons, we use a slowness of 0.26 s/km for the entire dataset. Previous work by *Cleveland and Ammon* [2013] focused only on improved locations of near vertical strike-slip earthquakes. As an extension to development of the relocation methods, we explore application of the method to linking strike-slip and normal faulting events.

4. Relative Relocation Results for the Northeast Pacific

4.1 Earthquake Relocations

Our improved relative locations are displayed in Figure 3 and listed in Table S1. Our relative locations within each earthquake cluster are precise, but the entire cluster can be shifted. If there is a regional bias in the original event locations, as has been noted for events in this study region (e.g. *Dziak et al.*, 1991; *Cronin and Sverdrup*, 2003; *Braunmiller and Nábělek*, 2008), the relocated events inherit this bias. Ground truth information on one or more earthquakes could be used to compute absolute locations. While there have been ocean bottom seismometer studies in this region (i.e. *Sverdrup et al.*, 1985), unfortunately none include events common with this study. The event linking criteria separates the events into two groups, those in the Explorer Plate and those along and in the Blanco and Gorda Block.

45°-dipping normal faults does not introduce a source-related phase shift when the strikes

are parallel or orthogonal, allowing their cross-correlation to measure the locations-based

197

198

199

200

201

202

203

204

205

206

207

208

209

210

211

212

213

214

215

216

217

218

phase shift (see electronic supplement). Considering the acceptable range of focal parameters, we use the GCMT catalog to limit the included strike-slip events to those with null axis plunge of 70° to 90° and the normal faulting events with null and tension axis plunge of 0° to 20°. One must also be concerned about differences in strike, particularly when linking strike-slip and normal faulting events. Inspection of the included events showed that the normal faulting events have strikes nearly parallel or normal to the nearby strike-slip events. To insure that the mechanism differences do not affect the results, we estimated locations using only strike-slip events and using a combined data set including strike-slip and normal faulting events. Locations differences were minor (~5 km on average) between the inversions, providing confidence that linking with normal faulting events does not adversely effect event locations. Additionally, we visually analyzed all the azimuthal travel-time patterns corresponding to linked normal and strike-slip events, guided by the theoretical discussion and synthetic seismogram calculations. We did not observe appreciable azimuthal artifacts that would produce erroneous effect on the relocations. For all events, examination of the azimuth travel-time patterns did not indicate any nodal effects large enough to influence the relocations.

The distance between the initial epicenter and final epicentroid locations for all 161 events range from 0 to 69 km, with a median shift of about 12.9 km (Figure 4). The absolute value of the centroid time shifts for all events range from 0.01 to 9.37 s with a mean absolute shift of 2.08 s; the overall mean and median shifts are about 0.00 s and 0.05 s, respectively. Part of the centroid time shifts reflects the difference between time of initiation of rupture and the centroid time, which can (and should) be large for larger

220

221

222

223

224

225

226

227

228

229

230

231

232

233

234

235

236

237

238

239

events.

events. For most of the events, distance and time changes do not correlate. However, the events with the largest distance offsets also had large time changes. The Explorer events (those north of 46°N) have a median distance shift of 19.6 km and mean and median time shifts of 0.00 s and 0.36 s. The southern events have a median distance shift of 11.2 km and mean and median time shifts of 0.00 s and 0.03 s. As a whole, relocated events in the north moved a greater distance than those in the south. This difference is reflected in the two median distance shifts (~11.2 km in the south and ~19.6 km in the north). In the southern region, six events moved more than 25 km; twenty-eight moved more than this distance in the north. The three events in the south that moved the farthest were all located along the BTFZ (08 Aug 2012 17:45:33, M_w 4.9, moved 69.2 km; 10 Jan 2008 01:37:19, M_w 6.3, moved 54.6 km; and 27 Oct 1994 17:45:58, M_w 6.3, moved 47.6 km). The difference between epicenter and epicentroid could partly contribute to the distance moved in the two larger events. however, both the 2012 and 2008 events are more collinear with nearby events than their original locations. While the northern events had a higher median shift, only two events moved more than 40 km (11 Sept 2008 23:26:19, M_w 5.2, moved 56.3 km; and 14 Sept 2001 04:45:08, M_w 6.0, moved 40.4 km). The 2008 event moved to where a cluster of seismicity was consolidated by the relocation. The 2001 event is located in the region of diffuse seismicity of the Sovanco Fracture Zone. As with the events in the south, visual inspection of the observed azimuth travel-time patterns support the relocations for these

241

242

243

244

245

246

247

248

249

250

251

252

253

254

255

256

257

258

259

260

261

For those events in common, we compare our locations to those of other studies (Figures 5-7). To facilitate comparison, reduce possible regional bias in our work, and achieve values closer to absolute locations, we applied static shifts to our relative locations. Given the paucity of seismicity along the Juan de Fuca Ridge, seismicity around the Explorer Plate does not link with any BTFZ or Gorda seismicity; as a result there are no constraints on the relative locations between these regions. In the north, we follow the method of Braunmiller and Nábělek [2002] and fix the 06 April 1992 M_w 6.7 earthquake to the location carefully calculated by Cassidy and Rogers [1995] (50.55°N, -130.46°E); Cassidy and Rogers [1995] located the 1992 event using P- and S-wave travel-time residuals and corrected for regional bias using Wahlström and Rogers [1992]. Comparing our locations to those of Braunmiller and Nábělek [2002], we relocated eight events contained in this earlier study (Figure 5, Table S2). Excluding the 06 April 1992 event, the seven remaining events differ in location between the two catalogs by ~3.6 to 37.5 km, with a median difference of 10.4 km; there is no systematic difference in azimuth. The biggest difference between the two catalogs (37.5 km) was the 07 April 1992 00:42:21 earthquake. The relocation of *Braunmiller and Nábělek* moved this event over 77 km southwest of the NEIC location and over 30 km southwest of the closest relocated events. Our location aligns the 1992 event with the pattern of the surrounding events, providing confidence in our location. Other than the 07 April 1992 00:42:21 event, which Braunmiller and Nábělek [2002] located well west of the other events, Braunmiller and Nábělek's locations are generally in agreement with the trends that ours display.

263

264

265

266

267

268

269

270

271

272

273

274

275

276

277

278

279

280

281

282

283

In the south, we do not have a viable single event to use as an absolute reference location. Instead, we shift our BTFZ events 30 km at 200° azimuth, a minimal amount that appears to best correlate the seismic trend with the bathymetry (Figure 6). Similar shifts were applied by Cronin and Sverdrup [2003] (28 km at 186°) and Braunmiller and Nábělek [2008] (25 km at 212°). Other studies have used locations calculated using Tphase data to provide reference locations. Considering the influence bathymetry local to the source can have on these locations, we do not feel this method is necessarily any more accurate. For this region, we found four other catalogs with relocations of common events as ours. With the static shift applied, we find our locations provide the best agreement with the local variations in bathymetry. The general patterns are similar as those represented in Dziak et al. [2000] and Braunmiller and Nábělek [2008]; however, our observations locate the events along about half as narrow a band of seismicity than Braunmiller and Nábělek [2008]. The locations of Cronin and Sverdrup [2003] again display broader scatter in locations and only a general agreement with local bathymetry. We did not apply a static shift to the events in and around the Gorda block because the locations appear to correlate well with the Mendocino Transform Fault in the north-south direction and are about 20 km shifted east relative to the Gorda Rise (Figure 7). The azimuthal orientation of our normal faulting earthquake locations matches the bathymetric trend defining the Gorda Rise. The most comprehensive catalogs of earthquake relocations in this region predate the period of our catalog [Stoddard and Woods, 1990; Sverdrup, 1987], so we cannot compare similar events, however, the general seismicity patterns in these earlier studies appear to agree with our results. The

- 284 following sections provide a more detailed analysis of seismicity of the Gorda Block,
- 285 Blanco Transform Fault, and Explorer Plate.

4.2 The Gorda Block

The Gorda block is young oceanic lithosphere (≤ 5 Ma) [Stoddard and Woods, 1990] that subducts beneath Oregon and California. The Mendocino Transform Fault (MTF) provides the southern border and the Gorda Ridge (GR) the western. To the north is the BTFZ. The GR and MTF separate the Pacific Plate to the west and south from the Gorda block. In one model for the region, Riddihough [1980] identified three GR sections, each divided by small transforms [Chaytor et al., 2004]. Spreading rates of these sections range from 55 to 25 mm/yr and decrease toward the south [Riddihough, 1980]. Magnetic anomaly patterns provide evidence for recent and ongoing deformation within the Gorda Block (e.g. Menard and Atwater 1968; Atwater and Mudie, 1973; Riddihough, 1980, Carlson and Stoddard, 1981).

Our catalog of the Gorda intraplate seismicity is relatively sparse, and the relocations do not significantly change existing seismicity patterns, other than collapsing several of the events into a tighter cluster along the northern Gorda Ridge (assuming the event location offset from the ridge is a result of the initial location bias). While some locations move over 20 km, these do not significantly affect the tectonic interpretation that the Gorda block is long known to deform internally.

304

305

306

307

308

309

310

311

312

313

314

315

316

317

318

319

320

321

322

323

324

4.3 Blanco Transform Fault Zone

The Blanco Transform Fault Zone (BTFZ) is a strike-slip fault that extends ~360 km between the Gorda Ridge to the east and Juan de Fuca Ridge to the west (Figure 1). The BTFZ is commonly described as composed of five transform segments, separated by extension basins. These basins include the Gorda Depression, Cascadia Depression, Surveyor Depression, and East and West Blanco Depressions, [McManus, 1965; Embley et al., 1987]. The easternmost portion of the BTFZ is the Gorda Depression Segment. Earthquakes in this region are generally shallow (4-6 km) and small ($M_w \le 5.3$). Normal faulting is observed at the northern Gorda Ridge and within the Gorda Depression. Braunmiller and Nábělek [2008] calculated 15% seismic coupling for this segment. West of the Gorda Depression is the Cascadia Segment, which includes the Blanco Ridge and Cascadia Depression. In its eastern limit, the Blanco Ridge is the narrow, steep northern border of the Gorda Depression. With a ~150 km length, the 5 Ma Blanco Ridge [Embley and Wilson, 1992] is the longest uninterrupted ridge segment of the BTFZ. The peak seismic slip rates [Braunmiller and Nábělek, 2008] and largest recorded earthquake [Dziak et al., 1991] of the BTFZ occurred along the Blanco Ridge. Estimated average seismic coupling values along the entire BTFZ vary considerably (e.g. Hyndman and Weichert, 1983; Boettcher and Jordan, 2004; Willoughby and Hyndman, 2005; Braunmiller and Nábělek, 2008), including 10% [Boettcher and Jordan, 2004] to 36% [Braunmiller and Nábělek, 2008] seismic coupling. These differences reflect the calculation's dependence upon assumed vertical extent of seismogenic region and the assumed value of the shear rigidity. East of 127.9°W, the ridge is more seismically

326

327

328

329

330

331

332

333

334

335

336

337

338

339

340

341

342

343

344

345

346

active, including six of the ten $M_w \ge 6$ earthquakes recorded along the BTFZ [NEIC, GCMT], leading Braunmiller and Nábělek [2008] to describe this region as having full seismic coupling. Braunmiller and Nábělek [2008] describe lower seismicity rate and earthquake sizes west of 127.9°W and estimate the seismic coupling to be less than 50%. The Blanco Ridge segment terminates in the west along the southern border of the Cascadia Depression. Normal faulting seismicity is observed between 128.5° to 129.2°W in the Cascadia and Surveyor Depressions [Braunmiller and Nábělek, 2008]. The Surveyor Depression is located ~10 km northwest of the northwest corner of the Cascadia Depression. The seismicity along the Cascadia and Surveyor Segments is generally deep (6-9 km) and small (M_w ≤ 5.6). Braunmiller and Nábělek [2008] calculated 15% seismic coupling in these regions. The T-axis of the faults and geologic features suggest the Surveyor Depression is a pull-apart deformation and the Cascadia Depression is a spreading center [Braunmiller and Nábělek, 2008; Embley and Wilson, 1992]. The Cascadia Depression is believed to have formed 5 Ma when PAC-JDF plate motion changed from 100° to 110°E. The Surveyor Depression is significantly younger, 0.35 to 0.4 Ma [Embley and Wilson, 1992]. The westernmost portion of the BTFZ, the Western Blanco Segment, is structurally more complex than the eastern segments. Like the Surveyor Depression, this segment is believed to be younger, with reorganization 0.4 Ma [Embley and Wilson, 1992]. Seismicity is largely strike-slip and shallow (4-6 km) [Braunmiller and Nábělek, 2008]. Braunmiller and Nábělek [2008] calculated 33% coupling in the Western Blanco

348

349

350

351

352

353

354

355

356

357

358

359

360

361

362

363

364

365

366

367

368

Segment. In addition to the main fault along the north wall of the Western Blanco Depression, additional transform fault strands are proposed for this region (e.g. Embley and Wilson, 1992; Dziak et al., 2003; Dauteuil, 1995; Delaney et al., 1981). Braunmiller and Nábělek [2008] could not delineate these strands based on earthquake locations, but noted that slip vectors support the presence of three strands. Adding a collective shift to our BTFZ earthquake relocations results in a strong correlation between seismicity and bathymetry. The relocations for events along the BTFZ generally concentrate the set of events into a more compact linear feature, however, not all of the events arrange into a single line. The results support interpretations that multiple active fault segments constitute the plate boundary (e.g. Embley and Wilson, 1992; Dziak et al., 2003; Dauteuil, 1995; Braunmiller and Nábělek, 2008). We lack the number of events to delineate specific fault traces, but visual analysis of our measurements for particular event pairs confirms that the events are not collinear. We observe a greater variance in the location of seismicity normal to the fault zone along the west BTFZ than the east [Braunmiller and Nábělek, 2008]. The difference between the east and west BTFZ system might reflect an increased fault-system complexity of the west relative to the east. Considering that the western BTFZ could be up to 5 Ma younger than the eastern (i.e. Embley and Wilson, 1992), the fault-system complexity supports the idea that as a transform fault matures, slip localizes to fewer active parallel faults. Observing the recent seismicity through time (Figure 8), a noticeable difference in recent event magnitude and rupture behavior is apparent between western and eastern BTFZ. As mentioned earlier, the western half has ruptured in three M > 6.0 between 1965 and 2015,

370

371

372

373

374

375

376

377

378

379

380

381

382

383

384

385

386

387

388

389

390

while the eastern half has experienced seven (NEIC); the eastern half has also experienced larger events than the western. The east tends to rupture in single events, with little or no aftershock sequences. In the west, there have been possibly repeating swarm-type rupture events between -130°E to -129°E. These differences in rupture behavior might also reflect the maturing of a single dominant fault, enabling larger single ruptures. Normal faulting event locations in the middle of the fault zone coalesce into a tighter cluster, which is consistent with a visual inspection of the cross-correlations between these events. Our catalog does not include any normal faulting events in the eastern half of the BTFZ. In the original NEIC hypocenters, there is a noticeable seismicity gap that includes regions both east and west of the Cascadia Depression (Figure 6 and 8). The relocation of the 27 October 1994 (M_w 6.29; 43.75°N, -127.92°E) and 10 January 2008 (M_w 6.22; 43.77°N, -127.94°E) epicentroids place them over 40 km west of their original location and significantly closer to the Cascadia Depression. The similarity in locations, rupture parameters, and magnitudes suggest the 2008 event may be at least a partial reactivation of the structures involved in the 1994 event. Prior to 1994, there were two M_w 6.4 (GCMT) events in 1981 and 1985 that could be related to the same features. Two other strong events occurred in 2000 (M_w 6.0) and 2012 (GCMT: M_w 6.0). Our observations relocated the 2000 event ~ 30 km to the east of the NEIC location (43.65°N, -127.61°E). We did not include the 2012 event in the final inversion because the GCMT dip, 62°, of one of the nodal planes was outside our acceptable range, however, preliminary relocations placed it near the 2000 event, suggesting it's rupture could overlap that of the

392

393

394

395

396

397

398

399

400

401

402

403

404

405

406

407

408

409

410

411

412

2000 event. Boettcher and McGuire [2009] relocated the 1981, 1985, 1994, 2000 and 2008 events. This study concluded the 1981, 1994, and 2008 earthquakes were colocated, while the 1985 and 2000 events ruptured a similar region ~25 km east of the 1981/1994/2008 events. The original NEIC hypocenters suggest that the fault segment between -128.5°E to -127.75°E did not host any large events since 1981. Our relocations suggest that is not the case. If the 1994/2008 events ruptured the entire region between the Cascadia Depression and the 2000/2012 epicentroids, the 1994/2008 events could account for slip along ~60 km of the boundary. Below, we describe how we used modeling to estimate the rupture length and seismogenic zone width of the 1994 event. Estimating the length of moderate-size ruptures is difficult. We performed a limited test for a long, unilateral rupture along a transform fault by looking for directivity effects. We computed the relative amplitude of intermediate-period R1 waves for signals from the 1994 earthquake relative to signals from all nearby events. The results are displayed as a function of azimuth in Figure 9. The results are noisy, but show a systematic variation that resembles a sinusoid, which is not representative of differences in faulting geometry. Some of the scatter arises because the amplitude is a measure of the relative directivity between 1994 and each of the other events. We interpret the amplitude modulation to be the result of rupture directivity in the 1994 event. We can reproduce the pattern using fundamental-mode synthetic seismograms [Herrmann, 2002] corresponding to vertical strike-slip sources computed with a flat-layered, earth model adapted from the 0-20 Ma oceanic lithosphere model of Anderson and Regan [1983]. We model rupture directivity using superposition of a series of point sources spaced one-km apart and shifted in time

based upon the rupture speed (see Figures S1 and S2 in the electronic supplement for details on the rupture directivity modeling using synthetic waveforms).

The pattern reveals several aspects of the rupture behavior. Since the ratio is 1994 scaled by other events, the maximum amplitude value is in the 1994 rupture direction. In our bandwidth, increasing the rupture length or decreasing the rupture speed enhances the amplitude of the pattern. The observations suggest that the 1994 event ruptured to the northwest (Figure 9). *Braunmiller and Nábělek* [2008] also reported northwestward rupture directivity for this event. The best fit to the data is an azimuth of $\sim 282^\circ$; the 1994 event GCMT strike is 296°. The amplitudes vary by roughly \pm 30-40%. Synthetic modeling of the pattern suggests that the rupture was predominantly unilateral; bilateral rupture results in a distinct pattern inconsistent with the observations. We are unable to produce amplitudes close to those observed using unilateral rupture lengths shorter than 30 km. A 30 km northwestward rupture is consistent with aftershock locations for the 1994 event reported in *Dziak et al.* [2000]. To fit the observations with a length of 30 km requires a rupture speed near or less than 1 km/s, while a rupture length of 60 km, the entire width of the "gap," requires a rupture speed over 4 km/s.

Using relative magnitude calculations documented in [Cleveland and Ammon, 2015] and listed in Table S1, we estimate that the relative moments of the 1994 and 2008 events differ by about 10%, which is consistent with Boettcher and McGuire [2009]. If we assume the 2008 event is a repeat of the 1994 and there was no slip between events and each event released all the plate motion strain accumulated between the events, based on MORVEL [DeMets et al., 2010], the approximate seismic slip is ~64 cm (using

~49 mm/yr). Assuming a mean shear modulus of 44.1 GPa [Boettcher and Jordan, 2004], the approximate rupture area would be ~115 km². Assuming a unilateral rupture of 60 km would require the width of the fault to be ~2 km; a 30 km unilateral rupture would require a width ~4 km. Studies suggest 600°C defines the lower bound of the seismogenic zone in oceanic lithosphere [e.g. Abercrombie and Ekström, 2001; Roland et al., 2010]. Based on mineral properties, Roland et al. [2010] suggest that the upper bound corresponds to a temperature of about 350°C. With these thermal bounds, thermal modeling by Roland et al. [2010], predicts a near constant seismogenic zone width of ~4 to 5 km along the portion of the plate boundary ruptured in the 1994 earthquake. A half-space cooling model would predict a seismogenic width that varies from nearly zero in the west to over 5 km in the east. Our calculations suggest the rupture width could be even narrower than these models predict.

4.4 Explorer Plate

The Explorer Plate is located north of the Juan de Fuca Plate, separated by the Nootka Fault Zone. The Dellwood Knolls, Revere-Dellwood Transform Fault, Explorer Ridge, and Sovanco Transform Fault all separate the Explorer from the Pacific Plate [Bebel et al., 1992]. Like the Gorda block, the Explorer Plate experiences significant intraplate seismicity. However, unlike the Gorda, magnetic lineations do not indicate substantial internal deformation in the Explorer [Bebel et al., 1992]. Several studies (i.e. Hyndman et al., 1979; Riddihough, 1984; Botros and Johnson, 1988) propose that the Explorer separated from the Juan de Fuca at about 4 Ma with the creation of the left-lateral Nootka

457

458

459

460

461

462

463

464

465

466

467

468

469

470

471

472

473

474

475

476

477

Transform Fault. An independent Explorer Plate is necessary since 4 Ma to account for the differences in orientation between the Explorer and Juan de Fuca [Riddihough, 1984; Botros and Johnson, 1988]. Prior to the Explorer-Juan de Fuca split, the Juan de Fuca is estimated to have been subducting beneath North America at > 5 cm/yr at ~105° azimuth (at 50°N, -130°E). Following the breakup, the Explorer's motion is believed to have slowed to 3-4 cm/yr and rotated clockwise to 120° azimuth [Riddihough, 1984]. Since that time, the Explorer's convergence with North America has continued to slow and rotate to a present ≤ 2 cm/yr at 145° azimuth [Braunmiller and Nábělek, 2002]. Multiple hypotheses, including heightened buoyancy [Riddihough, 1984] and reduced slab pull forces [Braunmiller and Nábělek, 2002], have been proposed to explain the slowing and rotation of convergence. The current tectonic setting of the Explorer Plate remains controversial. In one model, the Explorer is an independent plate bordered by the Pacific, Juan de Fuca, and North American Plates [Riddihough, 1977; 1984]. Alternatively, based on analysis of seismicity and detailed bathymetry, several studies [Barr and Chase, 1974; Rohr and Furlong, 1995] proposed the eastern portion of the Explorer Plate is becoming coupled with North America, whereas the western is accreting to the Pacific. This model suggests the formation of a new Pacific-North American Plate transform boundary, splitting the Explorer Plate. GPS measurements in northern Vancouver Island [Dragert and Hyndman. 1995; Henton et al., 1996] support this interpretation. Initially, slip vector orientations of intraplate seismicity [Wahlström et al., 1990; Kreemer et al., 1998] and inversion of seismic strain distribution within the Explorer Plate [Kreemer et al., 1998] also supported

479

480

481

482

483

484

485

486

487

488

489

490

491

492

493

494

495

496

497

498

499

this interpretation, however, measurements leading to this conclusion were later shown to be erroneous by Braunmiller and Nábělek [2002]. Rohr and Furlong [1995] inferred that the new fault is forming as a result of a southern lengthening of Queen Charlotte Fault. This would result in the extinction of the Explorer Ridge as the Pacific Plate captures it. Braunmiller and Nábělek [2002] proposed a different interpretation of the seismicity. They believe the Explorer continues to move independently of North America and the Pacific. Ongoing adjustments along the southeastern Explorer-Pacific boundary to bring it in agreement with the Revere-Dellwood fault is resulting in the formation of a new transform fault, called the Southwest Explorer transform boundary, separating the southwest corner of the Explorer Plate from the rest of the plate, causing just this corner to become a part of the Pacific Plate. North of the Southwest Explorer transform boundary, however, Braunmiller and Nábělek [2002] do not recognize the formation of a new fault boundary and believe the Explorer continues to move independently. A key reason for this conclusion was that Braunmiller and Nábělek [2002] found the azimuth of slip vectors of earthquakes in this region are inconsistent with Pacific-North America motion; azimuths largely ranged between Riddihough's [1984] Pacific-Explorer motion (310°) and Pacific-North America motion (340°), with an average value of 323°. Additionally, Braunmiller and Nábělek [2002] point out that much of the seismicity considered intraplate by Rohr and Furlong [1995] is actually an artifact of systematic mislocation to the northeast of regional seismicity. Earthquake relocation by Braunmiller and Nábělek [2002] shifted the location of much of the seismicity to the expected plate boundaries.

501

502

503

504

505

506

507

508

509

510

511

512

513

514

515

516

517

518

519

520

521

Even with our improved relative locations, the Explorer region seismicity remains spatially complex – a mix of small clusters, linear trends, and regions of diffuse seismicity. The seismicity patterns displayed by our relocations are consistent with those of Braunmiller and Nábělek [2002], including the observation that initial locations are biased toward the northeast. Although not a new result, our work confirms earlier conjectures that the deformation of the Sovanco Fracture Zone (FZ) is diffuse and not simply a result of low-quality locations. Much of the seismicity in the Sovanco Fracture Zone is smaller than M 4.5, which is below the magnitude threshold used in this study. South of the Sovanco, two tight clusters of seismicity are observed near 47.75°N, -128.75°E and 48.25°N, -129°E, falling along short transform step-overs resulting from overlapping spreading segments of the northern Juan de Fuca ridge [Weekly et al., 2014]. Through the middle of the Explorer, from around 49°N, -129°E to 49.5°N, -128.75°E, eight events align linearly NE-SW with the relocations, a pattern not observed with the initial scattered locations. The earthquakes appear to align in two or more ~220° trending en-echelon, linear patterns, consistent with the strike of the events. This linear pattern of intraplate seismicity, not included in any of the current tectonic models, suggests northeast-southwest oriented internal deformation of the Explorer Plate, possibly delineating faults that accommodate some slip previously attributed solely to the Nootka Fault. Southeast of this trend, seismicity remains diffuse. North of 49.5°N, seismicity becomes generally more linear, however, remains diffuse in a cluster centered around 51°N. North of this region, the seismicity appears to extend to the west before bending back east and following the coast of Moresby Island, British

523

524

525

526

527

528

529

530

531

532

533

534

535

536

537

538

539

540

541

542

543

544

Columbia, Canada. This linear pattern was also observed in Braunmiller and Nábělek [2002], however, our locations generally display ~ 10 km less scatter. Braunmiller and Nábělek [2002] noted that while seismicity through the Explorer and up to Oueen Charlotte Island roughly aligns with the direction of Pacific-North American plate motion, based on slip vectors they interpreted the seismicity as a series of right-stepping strike-slip faults as opposed to the formation of a new transform fault proposed by Rohr and Furlong [1995]. Our results do not support a simple through-going transform, and support the complex structure described by *Braunmiller and Nábělek* [2002]. North of ~ 51.25°N, our relocations do not follow the plate boundary inferred by the *Bird* [2003] model. Instead of stepping to the east, rupturing along the Queen Charlotte fault, seismicity appears to continue along a northern extension of the Revere-Dellwood fault (RDF). This is particularly true for the 17 November 2009 M_w 6.6 strike-slip earthquake, which displays a clear southwestern separation from the Oueen Charlotte fault by ~17 km. We also relocated two strike-slip events farther west of this RDF extension and the 2009 M_w 6.6 event, including an aftershock of this 2009 event (17 November 2009 M_w 5.8) and 17 June 2011 M_w 4.9. These locations are consistent with the tectonic model proposed by earlier studies (i.e. Braunmiller and Nábělek, 2002; Allan et al., 1993; Rohr, 2015; Rohr and Tryon, 2010), in which the RDF extends north to ~ 52°N, overlapping the Queen Charlotte fault by ~ 80 km. Seismic reflections presented in Rohr [2015] identify a second fault structure ~15 km southwest of the RDF extension. Our relocations display a southwest offset for these two smaller strike-slip events consistent with these structures. The M_w 6.6 mainshock triggered aftershock activity on the parallel fault to the southwest. The six northern-most normal faulting events we relocate are all aftershocks of the 2012

M_w 7.8 Haida Gwaii underthrusting earthquake. Based on slip models by *Lay et al.* [2013], these events are oceanward of peak slip regions of the 2012 rupture, likely indicating what can be viewed as typical outer rise responses to a large underthrust event.

5. Conclusions

545

546

547

548

549

550

551

552

553

554

555

556

557

558

559

560

561

562

563

564

565

566

We utilize cross-correlation of Rayleigh waves to calculate precise relative earthquake epicentroid locations in the northeast Pacific region. Our BTFZ relocations demonstrate the breadth (spread perpendicular to average strike) of the fault zone seismicity is more compact than initial locations. However, the seismicity does not collapse to a single trend, suggesting the presence of multiple active parallel faults along the fracture zone. The western and eastern BTFZ seismicity characteristics differ; seismicity is more scattered in the west, possibly relating to this portion of the fault being younger. We used directivity of the 27 October 1994 (M_w 6.29; 43.75°N, -127.92°E) earthquake along the BTFZ to constrain the rupture length to a range between 30-60 km. which when combined with a slip estimate based on plate rates suggests a narrow seismogenic zone width in the range of 2-4 km. The results are consistent with thermal bounds on OTF faulting. Relocations in and along the Explorer Plate identify a linear trend in seismicity north of ~49.5°N extending about 180-200 km to the north-northwest. North of ~51.25°N, seismicity pattern support models proposing northern extension of the Revere-Dellwood fault [Braunmiller and Nábělek, 2002; Allan et al., 1993; Rohr and Tryon, 2010], offset and overlapping the Queen Charlotte fault by ~80 km [Rohr, 2015]. South of ~49.5°N, seismicity within the Explorer is complex, reflecting evolving plate interactions. Our locations contain a SSW-NNE linear pattern of seismicity perpendicular

571

572

573

574

575

576

577

578

579

580

581

582

583

584

585

586

587

588

589

to the Sovanco Transform and extending 50 km into the Explorer Plate, possibly suggesting the development of a fault that accommodates some of the SSW-NNE slip previously attributed solely to the Nootka Fault.

Acknowledgments. This work was supported by the US Geological Survey and the Defense Threat Reduction Agency, under Award HDTRA1-11-1-0027. K.M.C. performed revisions of this work under the auspices of the Department of Energy for the Los Alamos National Laboratory under the contract DE-AC52-06NA25396. We acknowledge the staff and support provided to the IRIS/USGS GSN and Global Centroid-Moment-Tensor (CMT). Global Seismographic Network (GSN) is a cooperative scientific facility operated jointly by the Incorporated Research Institutions for Seismology (IRIS), the United States Geological Survey (USGS), and the National Science Foundation (NSF). The facilities of the IRIS Data Management System, and specifically the IRIS Data Management Center, were used for access to waveform and metadata required in this study. The IRIS DMS is funded through the National Science Foundation and specifically the GEO Directorate through the Instrumentation and Facilities Program of the National Science Foundation under Cooperative Agreement EAR-1063471. Waveform data used in this study are available through the IRIS Data System, http://service.iris.edu/fdsnws/. The National Earthquake Management Information Center (NEIC) Advanced National Seismic System (ANSS) Comprehensive Catalog (ComCat) was searched using http://earthquake.usgs.gov/earthquakes/search/. The Global Centroid Moment Tensor Project (GCMT) database was searched using www.globalcmt.org/CMTsearch.html. We also thank all those who openly share largeearthquake data recorded on their seismic networks. Thanks also to Bob Herrmann for

developing and sharing his Computer Programs in Seismology package, as well to the developers of SAC [Goldstein, et al., 2002] and GMT [Wessel and Smith, 1998]. We also thank Kevin Furlong for discussions of the results. Finally, we thank Jochen Braunmiller and Margaret Boettcher for their constructive criticism that greatly improved this paper.

References

22387.

590

591

592

593

594

600

- Abercrombie, R.E. and G. Ekström (2001), Earthquake slip on oceanic transform faults, *Nature*, **410** (6824), 74-77.
- Allan, J.F., R.L. Chase, B. Cousens, P.J. Michael, M.P. Gorton, and S.D. Scott (1993)

 The Tuzo Wilson Volcanic Field, NE Pacific: Alkaline volcanism at a complex,

 diffuse, transform-trench-ridge triple junction, *J. Geophys. Res.*, **98** (B12), 22367-
- Anderson, D.L. and J. Regan (1983), Uppermantle anisotropy and the oceanic lithosphere, *Geophys. Res. Letters*, **10** (9), 841-844.
- Atwater, T. (1989) Plate tectonic history of the northeast Pacific and western North

 America, in The Geology of North America, vol. N, *The Eastern Pacific Ocean*and Hawaii, edited by E. L. Winterer, D. M. Hussong, and R. E. Decker, pp. 21–

 72, Geol. Soc. of Am., Boulder, Colo.
- Atwater, T and J.D. Mudie (1973), Detailed near bottom geophysical study of the Gorda Rise, *J. Geophys. Res.*, **78**, 8665-8686.

609 Barmin, M.P., A.L. Levshin, Y. Yang, and M.H. Ritzwoller (2011), Epicentral location 610 based on Rayleigh wave empirical Green's functions from ambient seismic noise, 611 Geophys. J. Int., 184 (2), 869-884. 612 Barr, S.M. and R.L. Chase (1974), Geology of the northern end of the Juan de Fuca Ridge and sea-floor spreading, Can. J. Earth Sci., 11, 1384–1406. 613 614 Bebel, D.J., P.R. Stoddard and M.T. Woods (1992), A comparison of epicenter relocation 615 techniques: a case study for the Juan de Fuca plate, Physics of the Earth and 616 *Planetary Interiors*, **75**, p 25-38. 617 Behn, M.D., M.S. Boettcher, and G. Hirth (2007), Thermal structure of oceanic transform 618 faults, Geology, **35**, 307–310, doi:10.1130/G23112A.1. 619 Bergman, E.A. and S.C. Solomon (1988), Transform fault earthquakes in the north 620 Atlantic: Source mechanisms and depth of faulting, J. Geophys. Res., 93, 9027– 621 9057, doi:10.1029/JB093iB08p09027. Bird, P., Y.Y. Kagan, and D.D. Jackson (2002), Plate tectonics and earthquake potential 622 623 of spreading ridges and oceanic transform faults, in Plate Boundary Zones, Geodyn. Ser, vol. 30, edited by S. Stein and J. T. Freymueller, pp. 201–218, 624 AGU, Washington, D. C. 625 626 Bird, P. (2003), An updated digital model of plate boundaries, Geochemistry, 627 Geophysics, Geosystems, 4(3), doi: 10.1029/2001GC000252

628 Boettcher, M.S. and T.H. Jordan (2004), Earthquake scaling relations for mid-ocean ridge 629 transform faults, Journal of Geophysical Research, 107(B12302), 630 10.1029/2004JB003110 631 Boettcher, M.S., G. Hirth, and B. Evans (2007), Olivine friction at the base of oceanic seismogenic zones, Journal of Geophysical Research, 112(B1), p B01205, 632 633 doi:10.1029/2006JB004301 634 Boettcher, M.S. and J.J. McGuire (2009), Scaling relations for seismic cycles on mid-635 ocean ridge transform faults, Geophysical Research Letters, 36(21), p. L21301, 636 doi:10.1029/2009GL040115. 637 Botros, M. and H.P. Johnson (1988), Tectonic evolution of the Explorer-northern Juan de 638 Fuca region from 8 Ma to the present, J. Geophys. Res., 93, 10,421–10,437. 639 Braunmiller J. and J. Nábělek (2002), Seismotectonics of the Explorer region, Journal of 640 Geophysical Research, 107(B10), p. 2208, doi:10.1029/2001JB000220 Braunmiller J. and J. Nábělek (2008), Segmentation of the Blanco Transform Fault Zone 641 642 from earthquake analysis: Complex tectonics of an oceanic transform fault, 643 Journal Research, **113**(B7), B07108, of Geophysical p. 644 doi:10.1029/2007JB005213 645 Brune, J.N. (1968), Seismic moment, seismicity, and rate of slip along major fault zones, 646 *J. Geophys. Res.*, **73**, 777 – 784, doi:10.1029/JB073i002p00777.

647 Carlson, R.L. and P.R. Stoddard (1981), Deformation of the Gorda plate: A kinematic 648 view (abstract), EosTrans. AGU, 62, 1035. 649 Cassidy, J.F. and G C. Rogers (1995), The rupture process and aftershock distribution of 650 the 6 April 1992 MS 6.8 earthquake, offshore British Columbia, Bull. Seismol. 651 Soc. Am., **85**, 716–735. 652 Chaytor, J.D., C. Goldfinger, R.P. Dziak, and C.G. Fox (2004), Active deformation of the 653 Gorda plate: Constraining deformation models with new geophysical data, 654 Geology, 32 (4), 353-356, doi: 10.1130/G20178.2. 655 Cleveland, K.M. and C.J. Ammon (2013), Precise relative earthquake location using 656 surface waves, J. Geophys. Res. Solid Earth, 118 (1-12), doi: 10.1002/jgrb.50146. 657 Cleveland, K.M. and C.J. Ammon (2015), Precise Relative Earthquake Magnitudes From 658 Cross Correlation, Bull. Seismol. Soc. Am., 105 (3). 659 Cronin, V.S. and K.A. Sverdrup (2003), Multiple-event relocation of historic earthquakes 660 along Blanco Transform Fault Zone, NE Pacific, Geophysical Research Letters, 661 **30**(19), doi:10.1029/2003GL018086 662 Dauteuil, O. (1995), Fault pattern from SeaBeam processing: The western part of the 663 Blanco fracture zone (NE Pacific), Mar. Geophys. Res., 17, 17-35, 664 doi:10.1007/BF01268049. 665 Davies, G.F. and J.N. Brune (1971), Regional and global fault slip rates from seismicity, 666 Nature Phys. Sci., 229, 101–107.

667 Delaney, J.R., H.P. Johnson, and J.L. Karsten (1981), The Juan de Fuca ridge-hot spot-668 propagating rift system: New tectonic, geochemical, and magnetic data, J. 669 Geophys. Res., 86, 11,747–11,750, doi:10.1029/JB086iB12p11747. 670 DeMets, C., R.G. Gordon, and D.F. Argus (2010), Geologically current plate motions, 671 Geophysical Journal International, 181(1), p. 1-80, doi: 10.1111/j.1365-672 246X.2009.04491.x 673 Dragert, H. and R. D. Hyndman (1995), Continuous GPS monitoring of elastic strain in 674 the northern Cascadia subduction zone, *Geophys. Res. Lett.*, **22**, 755–758. 675 Dziak R.P., C.G. Fox, and R.W. Embley (1991), Relationship between the seismicity and geologic structure of the Blanco Transform Fault Zone, Marine Geophysical 676 677 Researches, 13(3), p 203-208. 678 Dziak R.P., C.G. Fox, R.W. Embley, J.L. Nábělek, J Braunmiller, and R.A. Koski (2000), 679 Recent tectonics of the Blanco Ridge, eastern Blanco Transform Fault Zone, 680 *Marine Geophysical Researches*, **21**, p 423-450. 681 Dziak, R.P., W.W. Chadwick Jr., C.G. Fox, and R.W. Embley (2003), Hydrothermal 682 temperature changes at the southern Juan de Fuca Ridge associated with Mw 6.2 683 Blanco Transform earthquake, Geology, 31(2), p 119-122 684 Dziewonski, A.M., T. Chou, and J. Woodhouse (1981), Determination of earthquake 685 source parameters from waveform data for studies of global and regional 686 seismicity, J. Geophys. Res., 86 (B4), 2825-2852.

687 Ekström, G. (2006), Global detection and location of seismic sources by using surface 688 waves, Bull. Seismol. Soc. Am., 96 (4a), 1201-1212, doi: 10.1785/0120050175. 689 Ekström, G. (2011), A global model of Love and Rayleigh surface wave dispersion and 690 anisotropy, 25-250 s, Geophysical Journal International, 187, p. 1668-1686, doi: 691 10.1111/j.1365-246X.2011.05225.x. 692 Ekström, G., M. Nettles, and A.M. Dziewonski (2012), The global CMT project, 2004-693 2010: Centroid-moment tensors for 13,017 earthquakes, *Phys. Earth Planet Int.*, 694 **200-201**, 1-9. 695 Ekström, G. and P.G. Richards (1994), Empirical measurements of tectonic moment 696 release in nuclear explosions from teleseismic surface waves and body waves, 697 Geophys. J. Int., 117 (1), 120-140. 698 Embley, R.W., L. D. Klum, G. Massoth, D. Abbott, and M. Holmes (1987), Morphology, 699 structure and resonance potential of the Blanco Transform Fault Zone, in Geology 700 and Resource Potential for the Continental Margin of Western North America and 701 Adjacent Ocean Basins—Beaufort Sea to Baja California, Earth Sci. Ser., vol. 6, 702 edited by D. W. Scroll, A. Grantz, and J. G. Vetter, pp. 549–562, Circum-Pac. 703 Res. Counc., Houston, Tex. 704 Embley, R.W. and D.S. Wilson (1992), Morphology of the Blanco Transform Fault Zone 705 - NE Pacific: Implications for its tectonic evolution, Marine Geophysical 706 *Researches*, **14**(1), p 25-45

- Engebretson, D.C., A. Cox, and R.G. Gordon (1985), Relative motions between oceanic and continental plates in the Pacific Basin, *Spec. Pap. Geol. Soc. Am.*, **206**, 59.
- Engeln, J.F., D.A. Wiens, and S. Stein (1986), Mechanisms and depths of Atlantic
 transform earthquakes, *J. Geophys. Res.*, 91, 548 577,
 doi:10.1029/JB091iB01p00548.
- Frohlich, C. and K. D. Apperson (1992), Earthquake focal mechanisms, moment tensors, and the consistency of seismic activity near plate boundaries, *Tectonics*, **11**(2), 279–296.
- Goldstein, P., D. Dodge, M. Firpo, and L. Minner (2002), SAC2000: Signal processing and analysis tools for seismologists and engineers, in *IASPEI International Handbook of Earthquake and Engineering Seismology*, edited.
- Henton, J.A., H. Dragert, R.D. Hyndman, M. Schmidt, P. Flueck (1996), Recent crustal deformation constraints for modelling the locked portion of the Cascadia subduction zone. *EOS Trans. AGU*, **77** (46), 147–148.
- Herrmann, R.B. (2002), Computer Programs in Seismology: An overview of synthetic seismogram computation.
- Herrmann, R.B., H. Benz, and C.J. Ammon (2011), Monitoring the earthquake source process in North America, *Bull. Seismol. Soc. Am*, **101** (6), 2609-2625.
- Hyndman, R.D., R.P. Riddihough, and R. Herzer (1979), The Nootka Fault Zone a new
 plate boundary off western Canada, Geophys. J. R. ast. Soc., 58, 667-683.

- Hyndman, R.D., and D.H. Weichert (1983), Seismicity and rates of relative motion on the
- plate boundaries of western North America, Geophys. J. R. Astron. Soc., 73, 59–
- 729 82.
- 730 Kawaski, I., Y. Kawahara, I. Takata, and N. Kosugi (1985), Mode of seismic moment
- release at transform faults, *Tectonophysics*, **118**, 313–327.
- 732 Kreemer, C., R. Govers, K.P. Furlong, and W.E. Holt (1998), Plate boundary
- deformation between the Pacific and North American in the Explorer region,
- 734 *Tectonophysics*, **293**(3-4), p 225-238.
- Lonsdale, P. (1991), Structural patterns of the Pacific floor offshore of Peninsular
- California, in Gulf and Peninsular Province of the Californias, edited by J. P.
- 737 Dauphin and B. R. T. Simoneit, *AAPG Mem.*, **47**, 87–143.
- 738 McGuire, J.J. (2008), Seismic cycles and earthquake predictability on East Pacific Rise
- 739 transform faults, *Bull. Seismol. Soc. Am.*, **98** (3), 1067–1084.
- 740 McManus, D.A. (1965), Blanco Fracture Zone, Northeast Pacific, Mar. Geol., 3, 429-
- 741 455, 1965.
- Menard, H.W. and Atwater, T. (1968), Changes in direction of sea floor spreading,
- 743 *Nature*, **219**, 463-467.
- Okal, E.A. and A.R. Langenhorst (2000), Seismic properties of the Eltanin transform
- 745 system, South Pacific, Phys Earth Planet Inter, 119, 185–208,
- 746 doi:10.1016/S0031-9201(99)00169-7.

- Riddihough, R.P. (1977), A model for recent plate interactions off Canada's west coast,
- 748 *Can. J. Earth Sci.*, **14**, 384–396.
- 749 Riddihough, R.P. (1980), Gorda plate motions from magnetic anomaly analysis, Earth
- 750 *Planet. Sci. Lett.*, **51**, 163–170.
- 751 Riddihough, R.P. (1984), Recent movements of the Juan de Fuca plate system, J.
- 752 Geophys. Res., **89**, 6980–6994.
- Rohr, K.M. and K.P. Furlong (1995), Ephemeral plate tectonics at the Queen Charlotte
- 754 triple junction, *Geology*, **23**(11), p. 1035-1038.
- 755 Rohr, K.M. and A.J. Tryon (2010), Pacific-North American plate boundary
- reorganization in response to a change in relative plate motion: Offshore Canada,
- 757 Geochem. Geophys. Geosyst., 11(6), Q06007, doi: 10.1029/2009GC003019.
- Rohr, K.M. (2015), Plate boundary adjustments of the southernmost Queen Charlotte
- 759 fault, *Bull Seism. Soc. Am.*, **105**(2B), doi: 10.1785/0120140162.
- Roland, E, M.D. Behn, and G Hirth (2010), Thermal-mechanical behavior of oceanic
- 761 transform faults: Implications for the spatial distribution of seismicity,
- Geochemistry Geophysics Geosystems, 11(7), Q07001, doi:
- 763 10.1029/2010GC003034
- Rundquist, D. and P. Sobolev (2002), Seismicity of mid-ocean ridges and its geodynamic
- implications: A review, Earth Sci. Rev., **58**, 143–161.

- Sobolev, P. and D.V. Rundquist (1999), Seismicity of oceanic and continental rifts—A geodynamic approach, *Phys. Earth Planet. Inter.*, **111**, 253 266.
- Stein, S. and M.E. Wysession (2003), *An Introduction to Seismology*, Earthquakes, and Earth Structure, 498 pp., Blackwell, Malden, MA.
- 770 Stock, J.M. and J. Lee (1994), Do microplates in subduction zones leave a geologic record?, *Tectonics*, **13**, 1472–1487.
- Stock, J.M. and P. Molnar (1988), Uncertainties and implications of the Cretaceous and
 Tertiary position of North America relative to Farallon, Kula, and Pacific plates, *Tectonics*, **6**, 1339–1384.
- Stoddard, P.R. and M.T. Woods (1990), Master event relocation of Gorda Block earthquakes: Implications for deformation, *Geophysical Research Letters*, **17**(7), p 961-964.
- Sverdrup, K.A. (1987), Multiple-event relocation of earthquakes near the Gorda Rise –
 Mendocino Fracture Zone intersection, *Geophysical Research Letters*, **14**(4), p
 347-350.
- Sverdrup, K.A., K.C. MacDonald, and W.A. Prothero (1985), Ocean bottom seismometer
 detection of earthquakes on the Gorda Rise near 41.5° north, *Marine Geophys*.
 Res., 7, 439-453.
- Turcotte, D. L. and G. Schubert (2002), *Geodynamics*, 2nd ed., Cambridge Univ. Press,
 New York.

- VanDeMark, T.F. (2006), Moderate and large earthquake activity along oceanic
- transform faults, MSc thesis, The Pennsylvania State Univ., 80 pp.
- 788 von Seggern, D. (1972), Relative location of seismic events using surface waves,
- 789 Geophys. J. R. ast. Soc., 26 (5), 499-513, doi:10.1111/j.1365-
- 790 246X.1972.tb05765.x.
- Waldhauser, F. and W.L. Ellsworth (2000), A double-difference earthquake location
- algorithm; method and application to the northern Hayward Fault, California,
- 793 Bull. Seismol. Soc. Am., **90** (6), 1353-1368.
- Wahlström, R. and G.C., Rogers (1992), Relocation of earthquakes west of Vancouver
- 795 Island, British Columbia, 1965-1983, Canadian Journal of Earth Sciences, 29(5),
- 796 953-961.
- 797 Wahlström, R., G.C. Rogers, and R.E. Baldwin (1990), P-nodal focal mechanisms for
- large earthquakes offshore Vancouver Island, Geol. Surv. Can. Open File Rep.,
- 799 2268.
- Weekly, R.T., W.S.D. Wilcock, D.R. Toomey, E.E.E. Hooft, and E. Kim (2014), Upper
- crustal seismic structure of the Endeavour segment, Juan de Fuca Ridge from
- traveltime tomography: Implications for oceanic crustal accretion, *Geochem*.
- 803 Geophys. Geosys., 15, 1296-1315, doi: 10.1002/2013GC005159 2014.

804	Wei, S., Z. Zhan, Y. Tan, S. Ni, and D. Helmberger (2012), Locating earthquakes with
805	surface waves and centroid moment tensor estimation, J. Geophys. Res., 117,
806	B04309, doi:10.1029/2011JB008501.
807	Wessel, P. and W.H.F. Smith (1998), New, improved version of Generic Mapping Tools
808	released, EOS, Trans. Amer. Geophys. U., 79, 579.
809	Wiens, D.A. and S. Stein (1983), Age dependence of oceanic intraplate seismicity and
810	implications for lithospheric evolution, J. Geophys. Res., 88, 6455-6468,
811	doi:10.1029/JB088iB08p06455.
812	Willoughby, E.C. and R.D. Hyndman (2005), Earthquake rate, slip rate, and the effective
813	seismic thickness for oceanic transform faults of the Juan de Fuca plate system,
814	Geophys. J. Int., 160, 855–868, doi:10.1111/j.1365-246X.2005.02523.x.
815	Wilson, D.S. (1986), A kinematic model for the Gorda deformation zone as a diffuse
816	southern boundary of the Juan de Fuca plate, J. Geophys. Res., 91, 10,259-
817	10,269.
818	Wilson, D.S. (1989), Deformation of the so-called Gorda plate, J. Geophys. Res., 94,
819	3065–3075.
820	

Figures

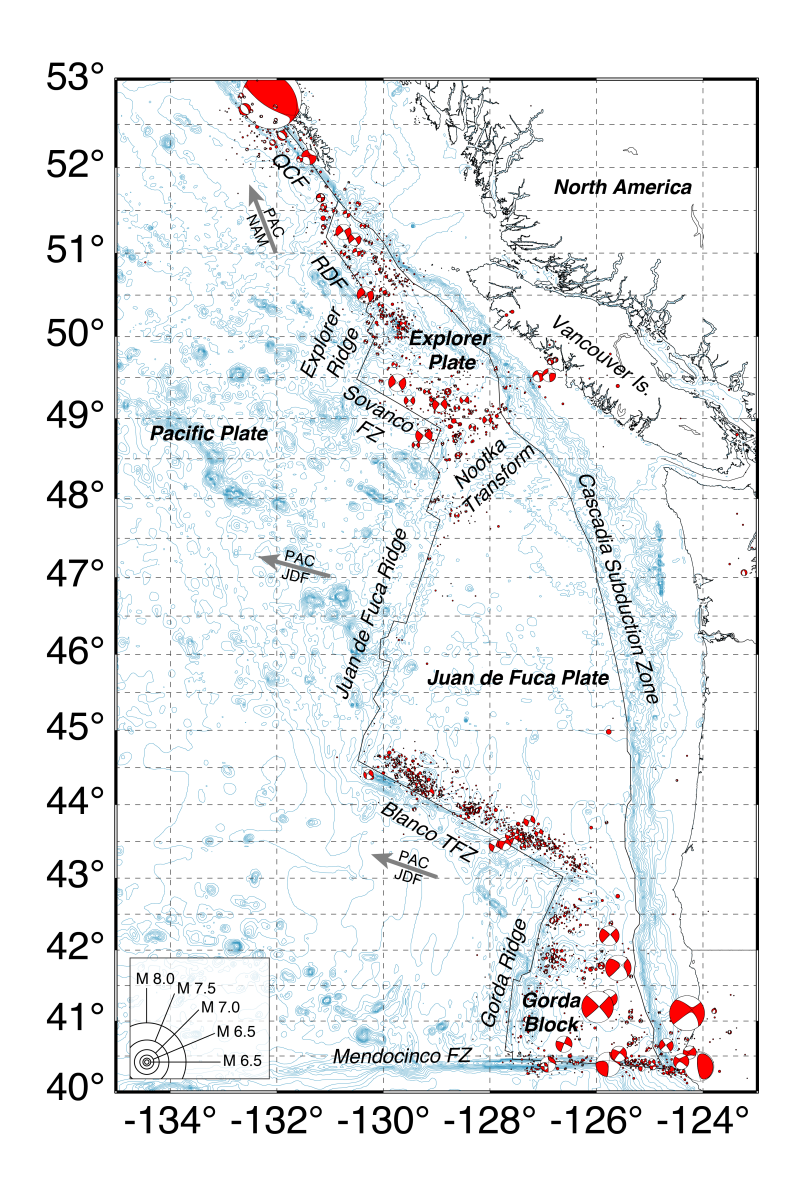


Figure 1: Regional seismicity of the northeast Pacific. Shown are locations and magnitudes of all events (including mechanisms) $M \ge 4.0$ in the NEIC catalog (since 1973). Focal mechanisms from the GCMT catalog are also shown for all events available. These mechanisms are located at the NEIC hypocenter and scaled in size according to NEIC magnitude. Plate motion directions are calculated using MORVEL [DeMets et al., 2010]. Plate boundaries (solid black line) are based on Bird [2003].

831

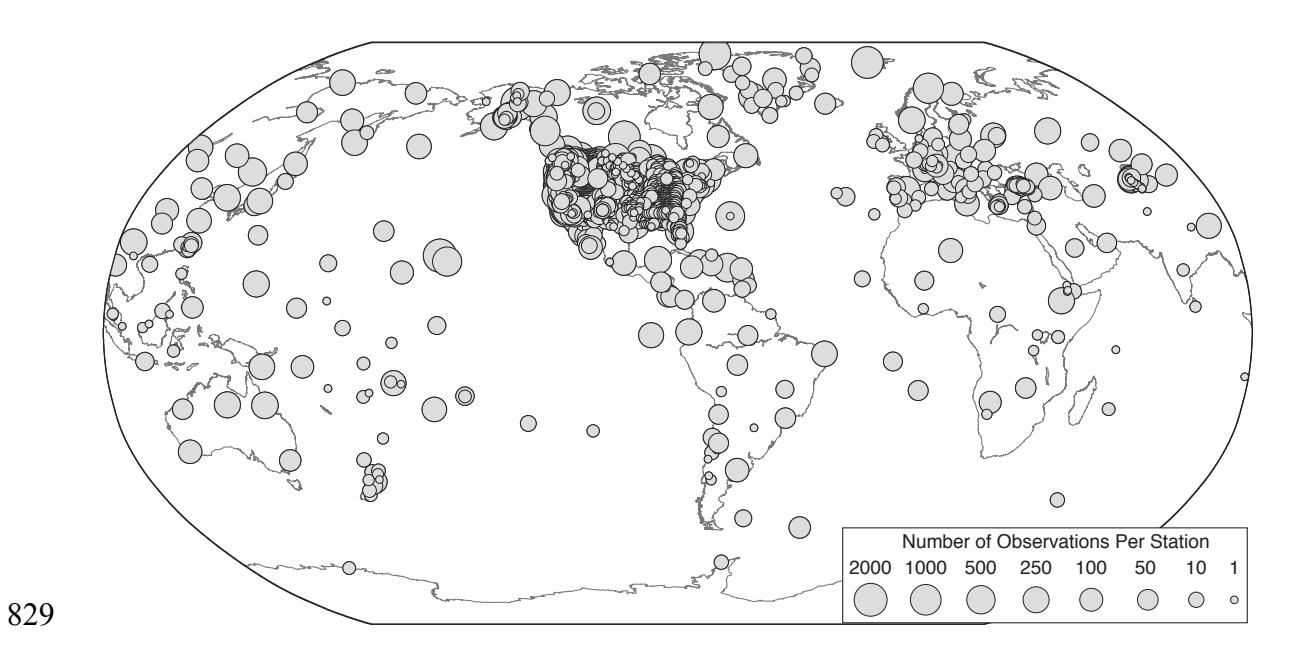


Figure 2: Locations of seismic stations used for relocation of earthquakes in this study.

The markers are scaled in size to the number of times waveforms from each station were used to calculate differential travel times between events.

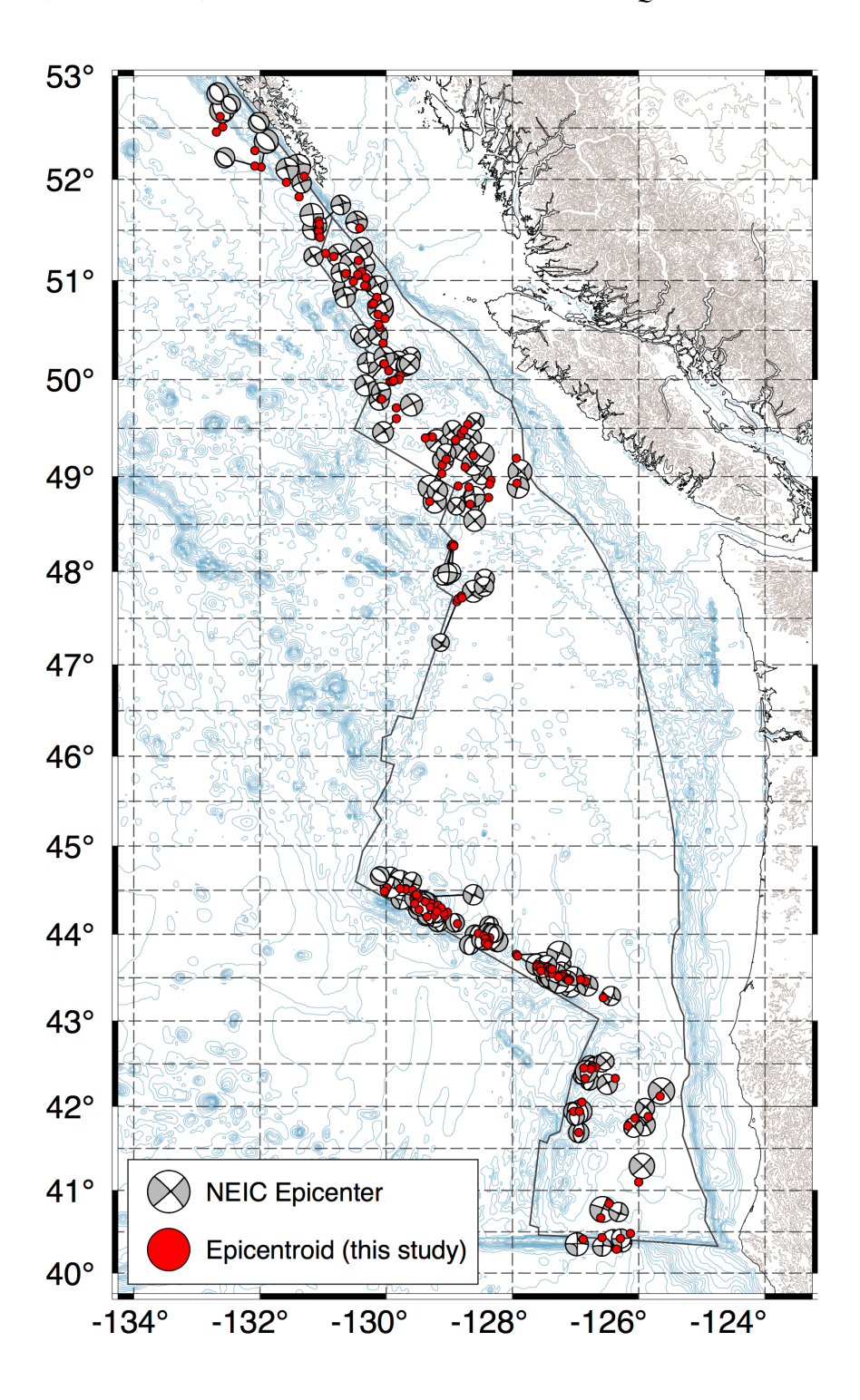


Figure 3: Relocated epicentroids from this study (red circle) compared to original NEIC locations (gray) labeled by the respective GCMT focal mechanism. Plate boundaries (solid black line) are based on *Bird* [2003].

839

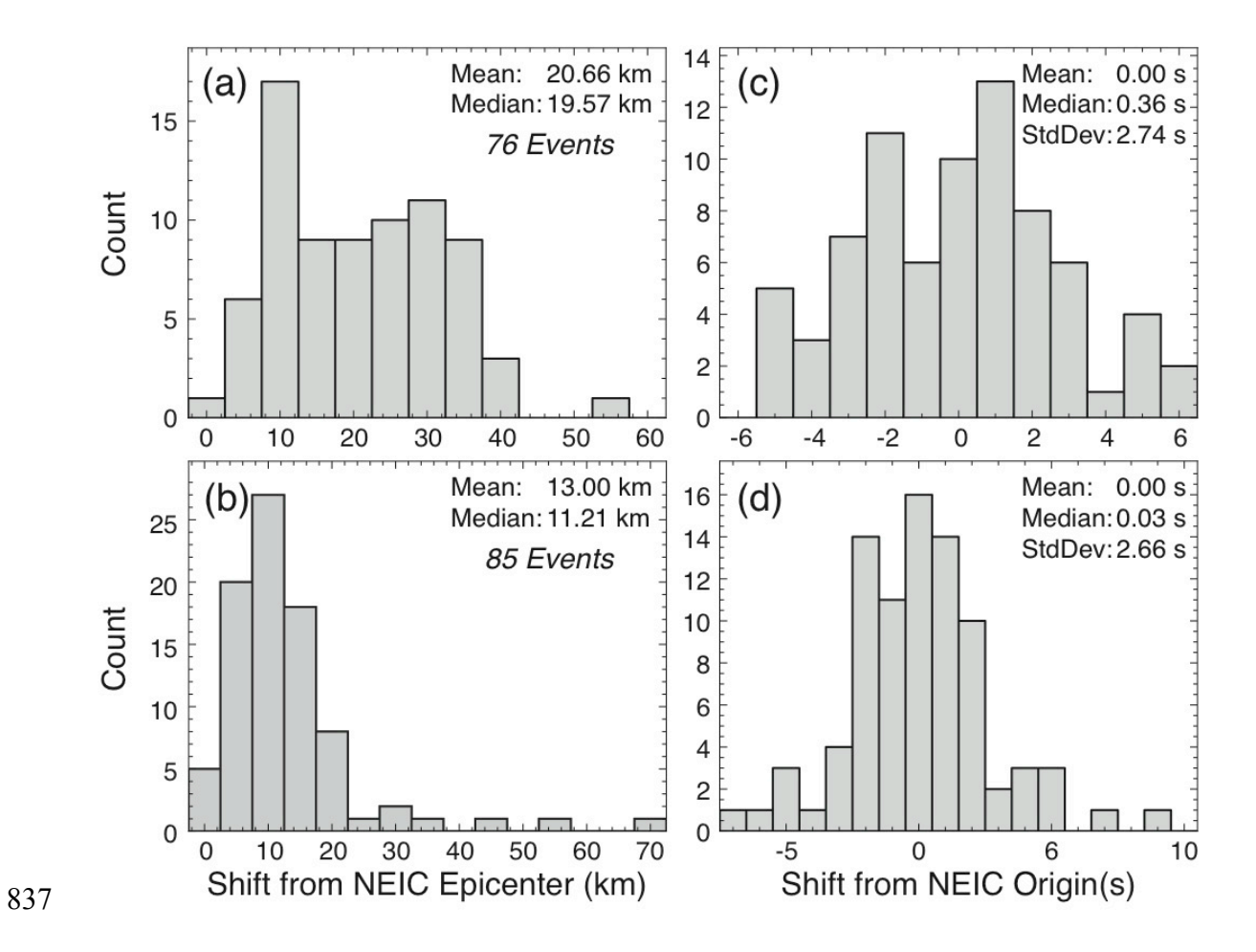


Figure 4: Comparison of the epicentroid locations with the original NEIC locations (subplots a and b) and origin time (subplots c and d) for events north (76 events, subplots a and c) and south (85 events, subplots b and d) of 46°N.

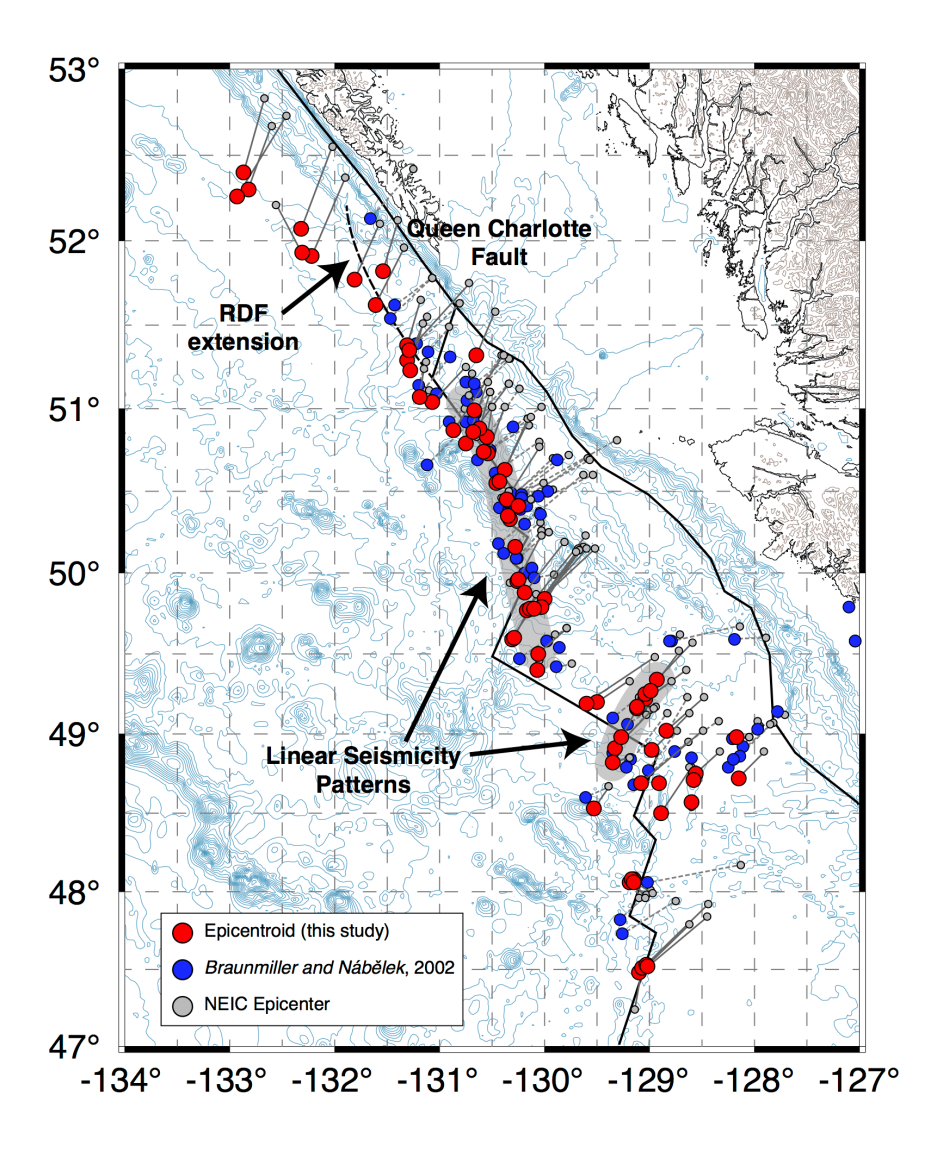


Figure 5: Explorer Plate relocated epicentroids from this study (red circle) compared to original NEIC locations (gray) and relocations from *Braunmiller and Nábělek* [2002] (smaller, blue). Following the method of *Braunmiller and Nábělek* [2002], we shift our relative relocations to fix the 06 April 1992 M_w 6.7 earthquake to the location carefully calculated by *Cassidy and Rogers* [1995] (50.55°N, -130.46°E). Plate boundaries (solid black line) are based on *Bird* [2003]. The dashed black line shows the proposed extension of the Revere-Dellwood fault (RDW) by *Rohr* [2015; *Rohr and Tryon*, 2010]. Highlighted in gray are two linear patterns observed in the improved seismic locations.

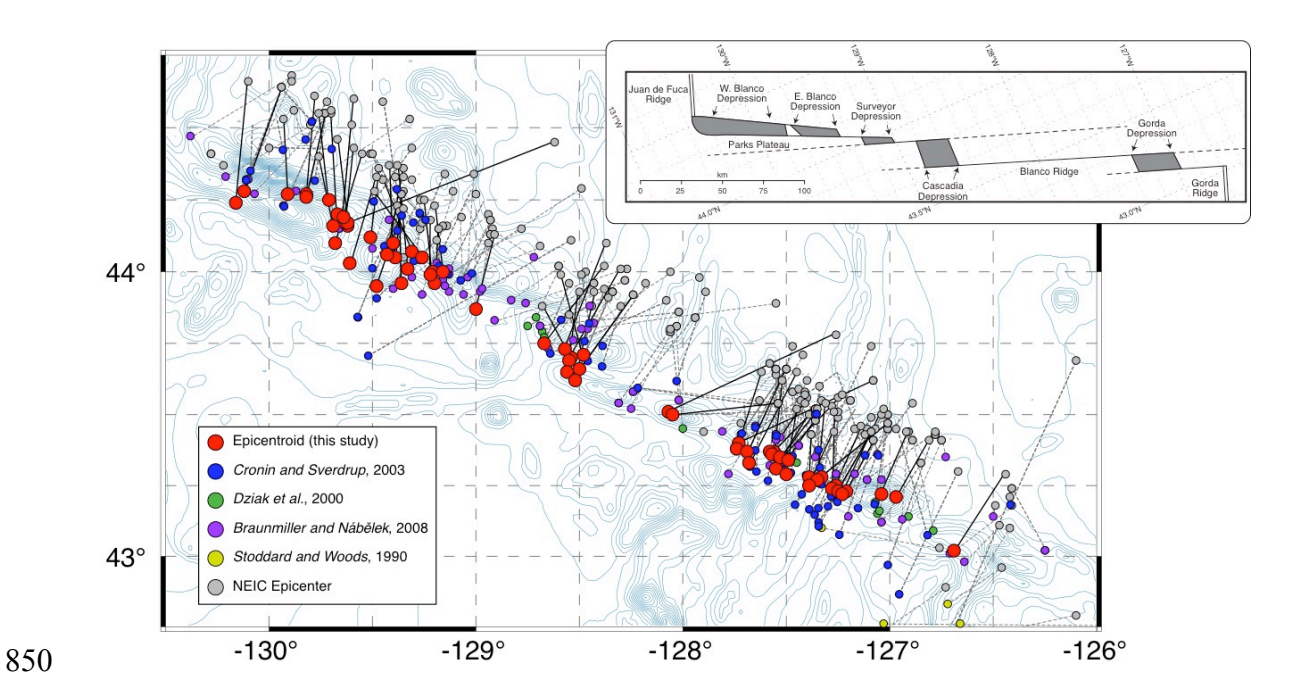


Figure 6: Blanco Transform Fault Zone relocated epicentroids from this study (red circle) compared to original NEIC locations (gray) and relocations from *Cronin and Sverdrup* [2003] (blue), *Dziak et al.* [2000] (green), *Braunmiller and Nábělek* [2008] (purple), and *Stoddard and Woods* [1990] (yellow). We shift our relative relocations a minimal amount that appears to best correlate with the bathymetry (30 km at 200° azimuth). The inset diagram is based on the bathymetry map in *Embley and Wilson* [1992].

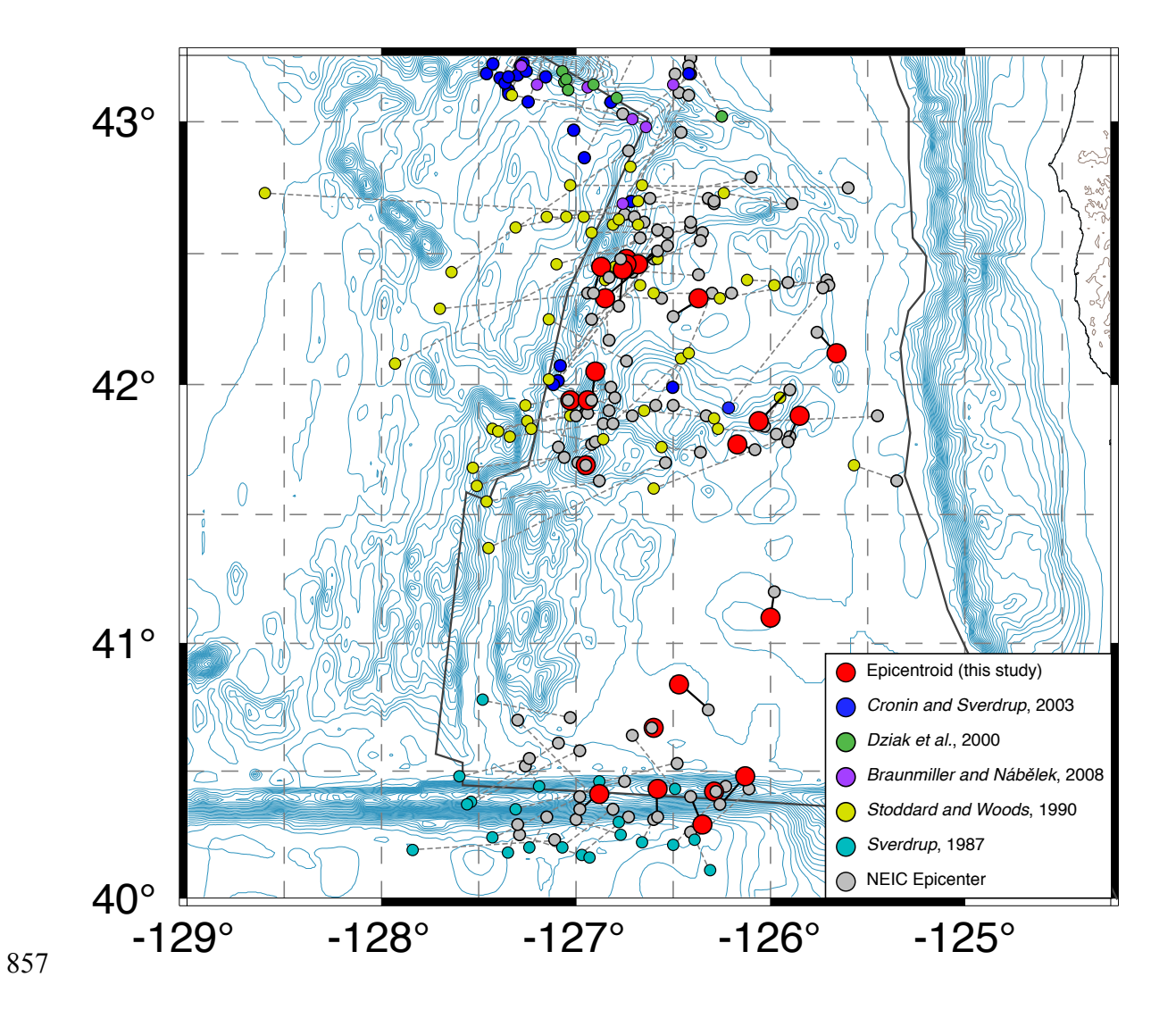


Figure 7: Gorda block relocated epicentroids from this study (red circle) compared to original NEIC locations (gray) and relocations from *Cronin and Sverdrup* [2003] (blue), *Dziak et al.* [2000] (green), *Braunmiller and Nábělek* [2008] (purple), *Stoddard and Woods* [1990] (yellow), and *Sverdrup* [1987] (light blue). There is no shift in our relative relocations. Plate boundaries (solid black line) are based on *Bird* [2003].

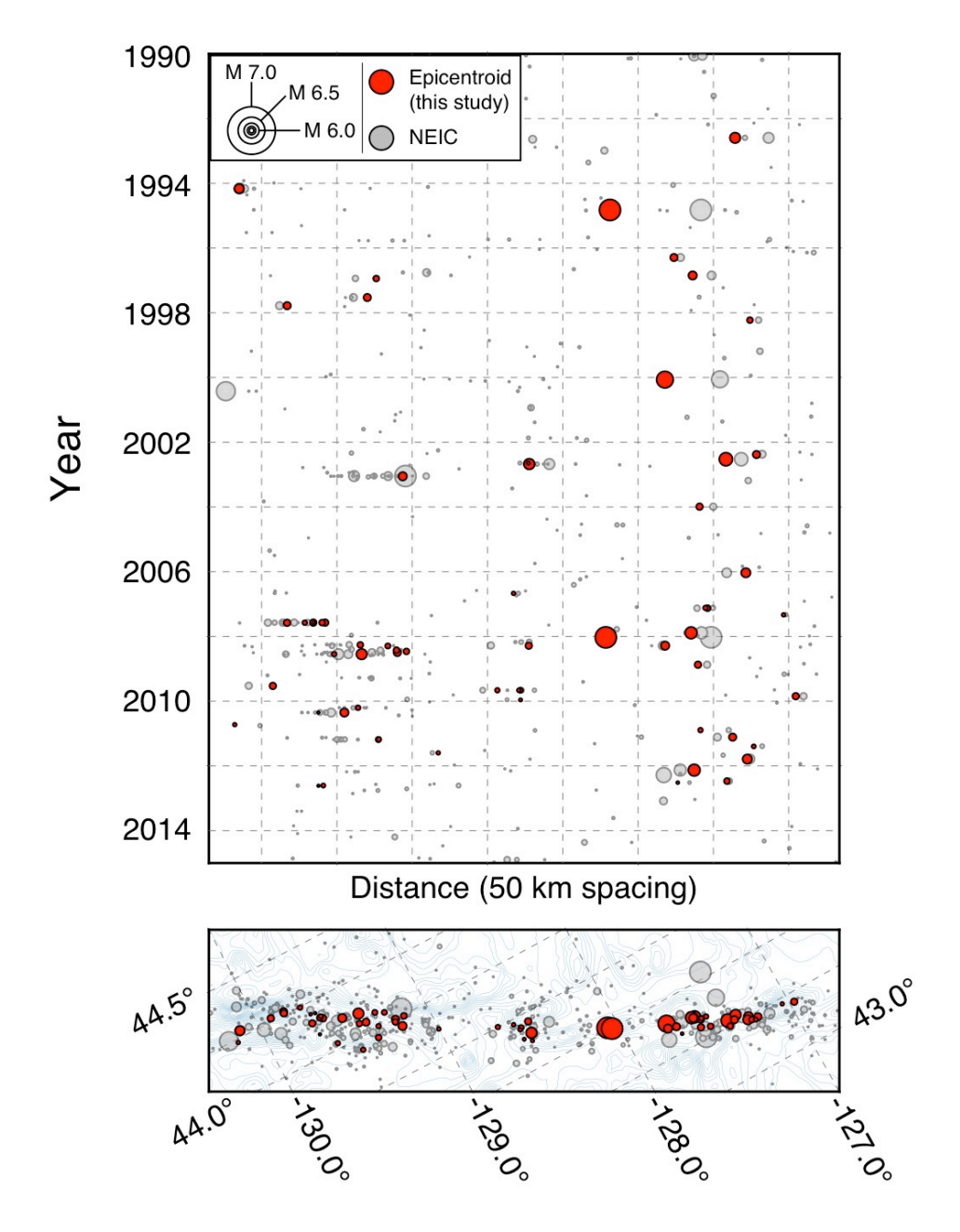


Figure 8: Timeline plot of Blanco Transform Fault Zone seismicity since 1992. Shown are both relocated epicentroids from this study (red) and all NEIC epicenters $M \geq 4.0$ (gray). A similar static shift as the relocated epicentroids (20 km at 200°) has been applied to the NEIC locations. Note differences in event locations are apparent, particularly for the large 1994, 2000, and 2008 events.

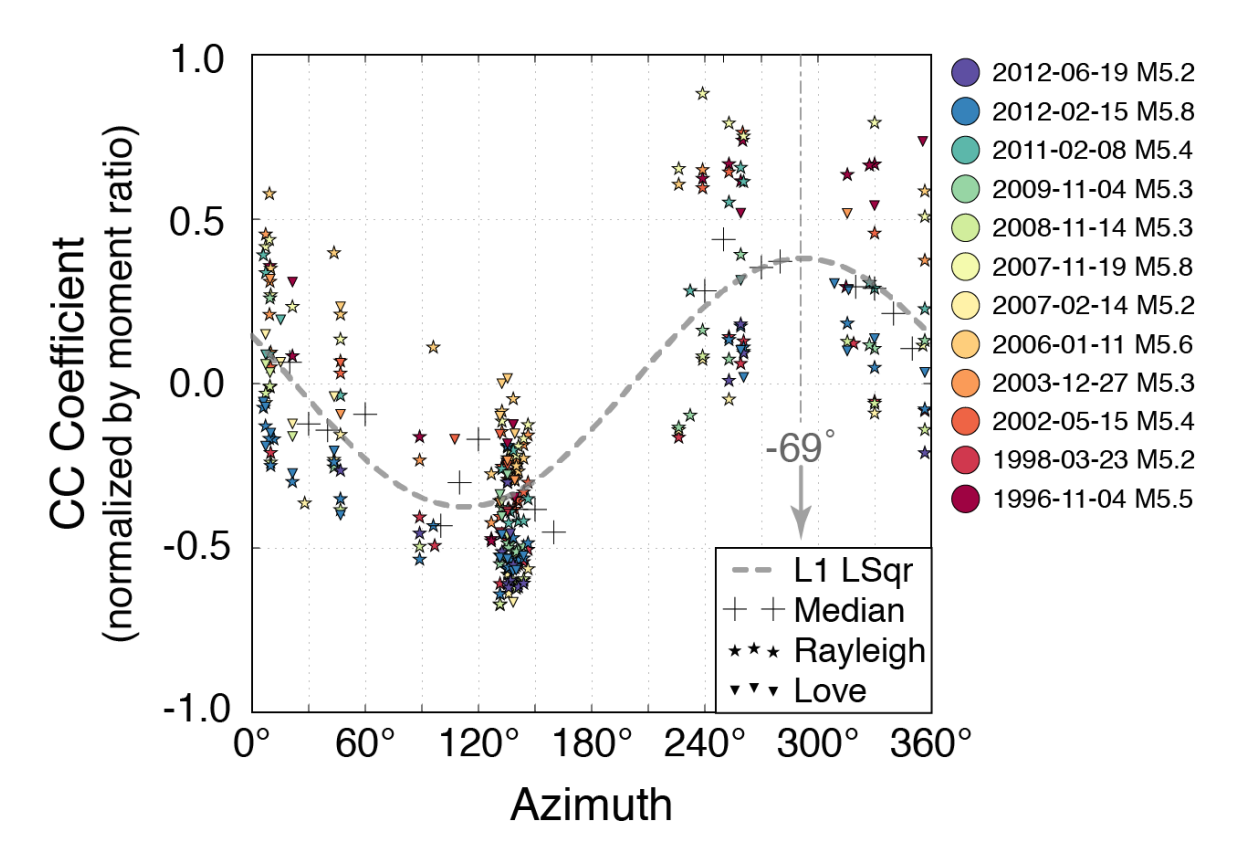


Figure 9: Unnormalized cross-correlation coefficient values (divided by the mean value and shifted to be centered at zero) between the 27 October 1994 $M_{\rm w}$ 6.3 Blanco Transform Fault Zone event and other surrounding events (labeled by color) at varying event to station azimuths. The observed cosine pattern (L1 optimized fit displayed with the gray, dashed line) results from rupture directivity of the 1994 event. The peak amplitude indicates the direction of rupture. Labeled is the observed strike of bathymetric ridges (-69°) [*Embley and Wilson*, 1992].

Tables (Electronic Supplement)

- 878 Table S1: Event relative relocations, shifted relocations and relative magnitudes.
- Table S2: Relocated events in common with earlier relocation studies.

Figures (Electronic Supplement)

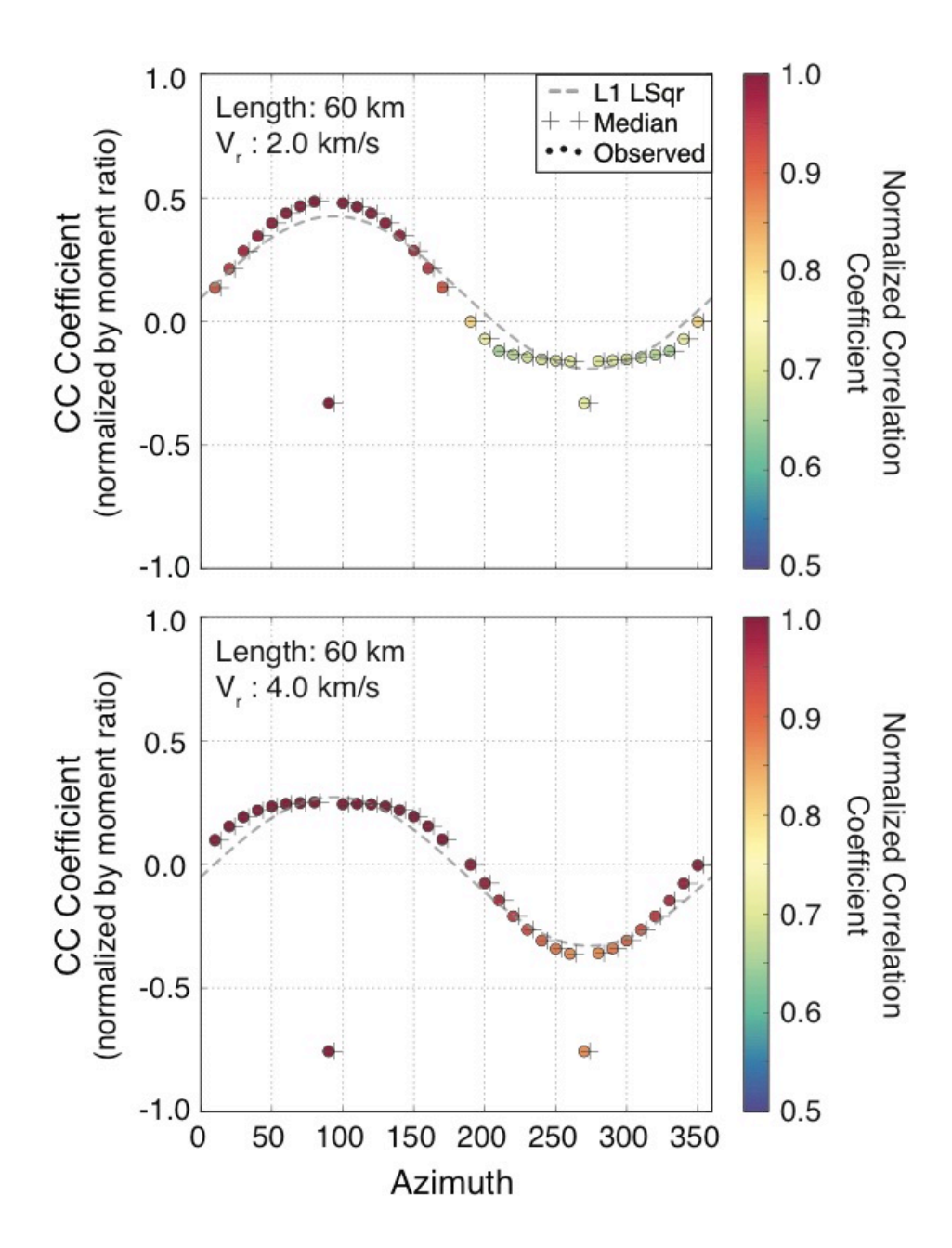


Figure S1: The cross-correlation coefficient normalized by moment ratio, at varying azimuths using synthetic waveforms (band 30 to 80 s). The master events are 60 km long in both examples, but the rupture speed varies (top: 2.0 km/s, bottom: 4.0 km/s). At lower speeds, the direction away from rupture (the tough) becomes flattened; the opposite pattern is observed at higher speeds.

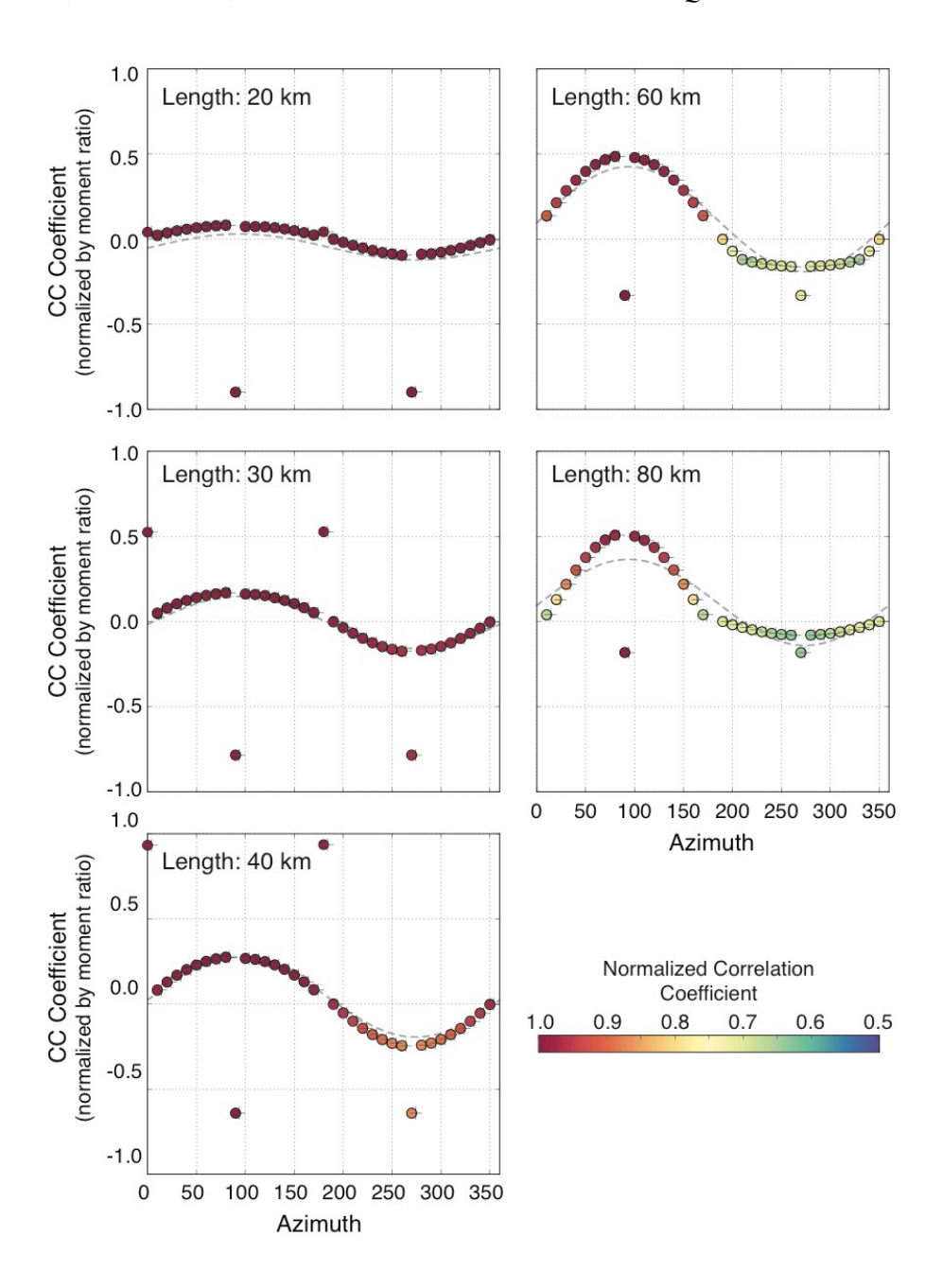


Figure S2: The cross-correlation coefficient normalized by moment ratio at varying azimuths using synthetic waveforms (band 30 to 80 s) with master events of varying length. All master events have a rupture speed of 2.0 km/s. At shorter lengths, the pattern is well described by a cosine function (gray, dashed line), but as the length increases, the peak (direction of rupture) becomes increasingly amplified while the opposite direction becomes flattened. Additionally, as the length increases the waveforms become increasingly dissimilar, particularly in the direction away from rupture; this is indicated by the systematic decrease in normalized correlation coefficient.